The Gelation of CAG Repeat Expansion RNAs Suppresses Global Protein Translation

Boxun Lu (luboxun@fudan.edu.cn)
Fudan University https://orcid.org/0000-0002-1675-9340
Yuyin Pan
Fudan University
Junmei Lu
Fudan University
Xinran Feng
Fudan University
Shengyi Lu
Fudan University
Yi Yang
University of Plymouth
Liang Wang
Tsinghua University
Pilong Li
Tsinghua University
Shouqing Luo
Plymouth University https://orcid.org/0000-0002-7998-3059

Biological Sciences - Article

Keywords: RNA molecules, eCAGr, global protein translation regulation, neurobiology

Posted Date: June 7th, 2021

DOI: https://doi.org/10.21203/rs.3.rs-541829/v1

The Gelation of Cytoplasmic CAG Repeat Expansion RNAs Suppresses Global Protein Translation

Abstract: RNA molecules with the expanded CAG repeat (eCAGr) may undergo liquid-to-gel phase transitions rapidly, but the nuclear eCAGr RNA foci display liquid-like properties, different from their gel-like behaviour *in vitro*[1]. The functional impact of this RNA gelation is also completely unknown[2]. Here we demonstrate that eCAGr RNA may form gel-like condensates (foci) in the cytoplasm that were rapidly degraded by lysosomes in a LAMP2-dependent manner. These RNA foci may lead to a drastic reduction of the global protein synthesis rate in cells and *in vitro*, possibly by sequestering the key protein translation elongation factor eEF2, which formed puncta colocalizing or surrounding the cytoplasmic eCAGr RNA condensates. Disrupting the eCAGr RNA gelation partially restored the global protein translation rate whereas the induction of enhanced gelation by an optogenetic system exacerbated this phenotype. Finally, eEF2 puncta were significantly enhanced in brain slices from a mouse model and patients of Huntington's disease, which is a CAG expansion disorder expressing eCAGr RNAs. Our study demonstrates the RNA gelation inside the cells and reveals its functional impact, providing new angles for understanding pathological mechanisms of repeat expansion diseases and global protein translation regulation.

Main Text:

Nucleotide repeat expansion is the common cause of many inherited diseases[3]. Among them, Huntington's Disease (HD) and certain types of spinocerebellar ataxias are caused by genes with expanded CAG repeat (eCAGr) sequences[4]. One of the most important questions in the field is why these diseases only manifest beyond a critical number of CAG repeats. Recent reports suggest that the eCAGr RNA undergoes liquid-liquid phase separation (LLPS) and possible phase transition (PT) into the gel-like phase, but the functional impact of the RNA LLPS and PT is completely unknown[1,2,5]. Identifying the functional role of RNA gelation may provide critical entry points to understand the pathological mechanisms of the diseases and possible physiological mechanisms of fundamental cellular functions.

Another intriguing observation in the previous reports is the inconsistency between the eCAGr RNA LLPS and PT in cells and *in vitro*: "Unlike their solid-like behaviour *in vitro*, CAG RNA foci in cells display liquid-like properties"[1]. While this was explained by the hypothesis that "the increased dynamicity might arise from specialized proteins in the nucleoplasm that remodel RNA base-pairing", it is still unclear why cytoplasmic eCAGr RNA foci are largely absent[1].

We speculated that eCAGr RNA LLPS and PT may have occurred in both the nucleus and the cytoplasm, but the cytoplasmic solid-like foci may have been cleared by lysosomal degradation, which is capable of degrading macroaggregates in the cells[6]. The nuclear eCAGr RNA foci may be less accessible to lysosomal degradation, so that they could be observed more tangibly.

In this study, we tested this hypothesis and observed lysosomal degradation-sensitive gel-like eCAGr RNA foci in the cytoplasm. We further investigated the functional role of the eCAGr

RNA LLPS and PT, and revealed its surprising effects in reducing the global protein synthesis rate through a novel mechanism.

Results

Observation of cytoplasmic eCAGr RNA foci

To visualize repeat-containing RNA foci in the cells, we utilized the previously established system by tagging the RNA with 12×MS2-hairpin loops and co-expressed yellow fluorescent protein (YFP)-tagged MS2-coat binding protein (MS2CP–YFP)[1]. Consistent with the previous report[1], we observed nuclear eCAGr (47×CAG) RNA condensates in HEK293T cells, whereas the short CAG repeat (12×CAG) RNA formed essentially no condensates (Fig. 1a). Similar to the previous report[1], very few cytoplasmic RNA foci were detected in any of the cells (Fig. 1a), suggesting that eCAGr RNA was unable to undergo LLPS and PT in the cytoplasm. This is counterintuitive, considering that eCAGr RNA alone was able to form solid-like "gels" *in vitro*[1]. The absence of cytoplasmic foci was also unlikely due to insufficient eCAGr RNA concentration in the cytoplasm, because the phenomenon was also observed in an exogenous over-expression system, in which the cytoplasmic eCAGr RNA concentration was high[1]. Thus, a more reasonable explanation is that the cytoplasmic eCAGr RNA foci may have been formed, but rapidly degraded in the cells *via* lysosomes, which are capable of degrading cytoplasmic RNAs[7,8], so that they could be hardly observed. To test this hypothesis, we treated the cells with lysosome inhibitors NH_4Cl or chloroquine (CQ), and observed numerous cytoplasmic RNA foci in most of the cells after the treatment (Fig. 1a-b). The presence and enrichment of cytoplasmic RNA foci could be caused by an enhancement of foci formation or an inhibition of foci degradation. Most of these foci colocalized with lysosomes (Fig. 1b), supporting the latter possibility. To further validate this, we performed live cell imaging and observed the emergence

of eCAGr RNA foci after adding the lysosome inhibitor NH_4Cl (Fig. 1c) as well as the disappearance of these foci after washing out NH_4Cl (Fig. 1d), confirming their lysosomal degradation. Finally, using the RNA fluorescence in situ hybridization (FISH) approach, we further confirmed the presence of cytoplasmic RNA foci in the HD mouse striatal ($STHdh^{Q7/Q111}$) cells expressing endogenous eCAGr RNA upon NH_4Cl treatment[9] (Fig. 1e).

LAMP2-depedent lysosomal degradation of cytoplasmic eCAGr RNA foci

The lysosomal degradation of cytoplasmic eCAGr RNA foci could be mediated by macroautophagy, an intracellular pathway in which autophagosomes engulf the cargoes and then fuse with lysosomes for degradation[10]. If this were the case, we would anticipate to observe substantial cytoplasmic eCAGr foci in macroautophagy-deficient cells (Atg5 knockout MEFs[11]) even without treatment of lysosome inhibitors. Surprisingly, the cytoplasmic RNA foci were still largely absent in the Atg5 knockout MEFs (Extended Data Fig. 1a), suggesting that they were cleared by macroautophagy-independent pathways. RNA molecules could also be degraded by lysosomes by RNautophagy, a cellular process in which the RNAs are loaded directly to the lysosomes by LAMP2[8]. Consistent with the involvement of RNautophagy, we knocked down LAMP2 (Extended Data Fig. 1b) and observed remarkable cytoplasmic eCAGr foci without treatment of lysosome inhibitors (47×CAG, Extended Data Fig. 1c). This was not observed when expressing short CAG RNA repeats (12×CAG, Extended Data Fig. 1c). Interestingly, none of the cytoplasmic eCAGr foci colocalized with lysosomes in the LAMP2 knock-down cells (Extended Data Fig. 1c), suggesting that they were not loaded to the lysosomes. Taken together, the cytoplasmic eCAGr RNA can form foci, which are rapidly degraded by lysosomes likely *via* LAMP2-dependent RNautophagy.

Cytoplasmic eCAGr RNA foci are solid-like condensates

We then investigated the physical properties of cytoplasmic versus nuclear RNA condensates. Consistent with previous studies[1], the nuclear condensates exhibited liquid-like properties as suggested by the near-complete fluorescence recovery after photobleaching (FRAP) (Fig. 1f & Supplementary Video 1). In contrast, cytoplasmic RNA condensates (foci) exhibited solid-like properties and there was essentially no recovery in the FRAP experiments for these foci (Fig. 1f & Supplementary Video 1), consistent with their properties *in vitro*[1]. Thus, the previously described RNA gelation observed *in vitro* actually occurred in the cytoplasm but not in the nuclei. These cellular RNA "gels" were not observed previously possibly because they were rapidly degraded by lysosomes (Fig. 1b).

The eCAGr RNA suppresses global protein translation

We then investigated the potential functional impact of these cytoplasmic eCAGr RNA gels. Changes of global protein translation rates have been recently reported in models of CAG repeat expansion disorders but remained controversial, with both upregulation and downregulation of global translation rates reported in different studies[12-17]. All these studies suggested or implied that the mutant protein with expanded polyQ is a major cause of the global protein translation change, but there has been a lack of proof. Knock-down experiments may reduce both eCAGr RNA and the polyQ protein, and thus cannot distinguish these two potential causes. Meanwhile, the *in vitro* translation experiments actually showed that addition of either the mutant protein with expanded polyQ or the wild-type protein with short polyQ reduced the translation rate to a similar degree[17], and the reduction might have been caused by the buffer of the purchased recombinant purified HTT proteins used in those experiments, because the buffer contained CHAPS, which is known to inhibit eIF4E translational activity[18]. Thus, we speculated

that the changes of global translation rates in those disorders might have been partially caused by the eCAGr RNAs.

We observed no significant changes in viability of HEK293T and STHdh cells expressing exogenous eCAGr RNAs from transfected plasmids (Extended Data Fig. 1d). Meanwhile, expression of the eCAGr RNA (72×CAG) led to an obvious decrease of the global protein synthesis rate, which was measured by the electrophoresis of nascent proteins at different time points using the Click-chemistry based metabolic labeling technique (Fig. 2a). Remarkably, eCAGr RNA expression for just 24 hours was sufficient to cause the reduction of global protein synthesis in HEK293T cells (Fig. 2b, *left*), suggesting that the effects are relatively rapid. We further confirmed this phenomenon in HD cells expressing endogenous eCAGr RNA, the $STHdh^{Q7/Q111}$ cells[9] (Fig. 2b, *right*). Noticeably, over-expression of the mutant *HTT* mRNA reduced global protein synthesis in the wild-type cells ($STHdh^{Q7/Q7}$) whereas knock-down of the *HTT* mRNA in the HD cells ($STHdh^{Q7/Q111}$) rescued this phenotype (Fig. 2c & Extended Data Fig. 2a), confirming that the phenomenon was caused by eCAGr RNA or its genetic products. Finally, to validate this effect at the single cell level, we performed high-content imaging analysis by a visualized global protein synthesis assay, and measured the protein synthesis of over 2,000 cells in each group, confirming the suppression of global protein synthesis caused by the expression of eCAGr RNA (Fig. 2d-e).

The reduction of global protein synthesis rate is likely due to deficits of global protein translation, which occur in several neurodegenerative disorders[19,20]. To confirm this, we transfected mRNAs encoding the renilla luciferase reporter protein in the cells and measured the protein translation rates by the luciferase signal (Fig. 2f). Consistent with the global protein synthesis assays, the translation of luciferase reporter protein was significantly reduced in cells

expressing endogenous eCAGr RNA (Fig. 2f). To exclude possible secondary effects in the cells, we further tested this effect in an *in vitro* protein translation system using the rabbit reticulocyte lysate. Pre-treatment of eCAGr RNA (72×CAG) but not the short CAGr RNA (25×CAG) for 5 minutes significantly reduced the translation of the luciferase reporter protein by the *in vitro* protein translation system (Fig. 2g), confirming the eCAGr RNA-mediated translation deficiency. The effects are likely mediated by the eCAGr RNA rather than its protein products, because the eCAGr RNA (72×CAG) has 6-stop codons before the CAG repeat, and is supposed to have little protein products based on literature[1]. In addition, the 36×CAG·CAA RNA that encodes the same amino acid sequence did not suppress protein translation (Fig. 2e&g). To further exclude the possibility of the involvement of the protein products from the repeat-associated non-ATG (RAN) translation, we expressed the RAN translation protein products in the cells, and observed no significant decrease in global protein synthesis (Extended Data Fig. 2b).

The RNA gelation is likely the major cause

While encoding the same amino acid sequence as the 72×CAG, the 36×CAG·CAA RNA did not suppress protein translation (Fig. 2e&g), possibly because the CAG·CAA mixture sequence may disrupt the formation of RNA LLPS and gelation[1,21]. Thus, the RNA gelation might be the fundamental cause of reduced global protein translation, possibly by sequestering certain key translation factors. To test this hypothesis, we disrupt the eCAGr RNA gelation by its previously reported binding oligonucleotide 8×CTG[1] or binding peptide BIND[22] without influencing the mHTT protein level (Extended data Fig. 3a-b). Transfection of 8×CTG or expression of BIND increased the global protein synthesis phenotype in the HD cells but not in the WT cells (Fig. 3a), suggesting that eCAGr RNA gelation is required for the reduction of

protein translation rates. This was further confirmed in the HEK293T cells expressing 72×CAG RNA versus the controls (Fig. 3b). To exclude possible secondary effects in the cells, we performed *in vitro* translation experiments and confirmed that the protein translation deficiency caused by eCAGr RNA could be restored by addition of BIND, probably through disruption of RNA gelation (Fig. 3c).

The RNA gelation-disruption experiments above confirmed the necessity of RNA gelation in regulating the global protein translation (Fig. 3a-c). In order to investigate the sufficiency of RNA gelation, we need to induce the RNA gelation and test the influence on global translation. Thus, we established an optogenetic system that allows us to induce the RNA LLPS and gelation by shining blue light on the samples (Fig. 3d), based on previous systems designed for protein LLPS and PT[23]. By conjugating the eCAGr RNA-binding peptide BIND to a blue-light sensitive protein CRY2, we managed to induce the clustering BIND-CRY2 by blue-light, leading to an increased clustering of eCAGr RNA (Fig. 3e) that colocalized with BIND-CRY2 *via* the protein-RNA interaction. The clustered eCAGr RNA became solid-like gels in the cytoplasm (Extended Data Fig. 3c), leading to a reduced global translation rate in the cells (Fig. 3f).

Taken together, we revealed the functional impact of eCAGr RNA gelation: reducing the global protein translation.

The eCAGr RNA regulates protein translation elongation

We then investigated the possible mechanism *via* which eCAGr RNA-mediated suppression of global protein translation. We performed the polysome profiling experiments to investigate the distribution of mRNAs with different numbers of ribosomes and observed only very subtle changes between HD and WT cells, or between cells expressing eCAGr versus the

controls (Extended Data Fig. 4a). This suggests that the translation defects are not due to ribosome assembly[24]. We further confirmed this by electrophoresis of total and cytoplasmic RNA, and qPCR detection of ribosome RNAs (rRNAs) including 45S, 28S and 5S, both of which did not exhibit any significant differences between HD and WT cells (Extended Data Fig. 4b-c), and the ribosome density seemed normal (Extended Data Fig. 4d). In addition, the nascent rRNA synthesis rate indicated by EU incorporation was similar in HD and WT cells (Extended Data Fig. 4e). Thus, the rRNA expression or assembly in HD cells was unlikely to be impaired.

To analyze the potential defects in translation machinery, we performed the SUnSET assay, which detects the total number of translating peptides at a specific time point by the C-terminus puromycin signals[25] (Extended Data Fig. 5a). The puromycin signals were not decreased but rather marginally increased in the HD cells (Extended Data Fig. 5a), suggesting that the number of translating peptides were not decreased. Meanwhile, the protein translation elongation impairment may not decrease the number of translating peptides and may increase their mature time (Extended Data Fig. 5b). This may explain why the SUnSET signals were not decreased. Consistent with this, knock-down of eEF2, a key translation elongation factor, also led to a marginal increase of SUnSET signals[26]. Thus, the SUnSET data suggest that the eCAGr RNA may impair the global protein translation elongation rather than initiation. A recent ribosome profiling study showed that the ribosome density distribution shifts towards the start and/or the stop codon in the HD cells[17], similar to eEF3 deficient yeast cells[27], and thus was consistent with the defects in translation elongation.

While the experiments above imply defects in the protein translation elongation, there has been a lack of direct evidence. Thus, we tested protein translation elongation directly by several published methods. We revealed the suppression of protein translation elongation in HD

cells by the SunRiSE (SUnSET-based Ribosome Speed of Elongation) assay, which measures the decrease of translating peptides when the translation initiation is blocked[28]. The HD cells exhibited a significantly slower decay of the SunRiSE signals, suggesting the impairment of protein translation elongation (Extended Data Fig. 5c). Finally, we characterized the translation elongation directly by the polysome run-off assay, which measures the polysome loss caused by translation elongation when the initiation is blocked[29]. The polysome run-off within 3 minutes was significantly reduced in the HD cells or the cells expressing 72×CAG RNA compared to the controls (Extended Data Fig. 5d), confirming the translation elongation impairment.

The eCAGr RNA foci induce the eEF2 clustering and degradation

Elongation factors such as eEF1 and eEF2 play a key role in protein translation elongation[30], and the observed defects in translation elongation could be explained by a lack of functional elongation factors. Consistent with this, the level of total eEF2 was decreased in the HD cells or cells expressing exogenous eCAGr RNA compared to the controls, whereas the level of eEF1A, the central functional component of eEF1 complex, was not influenced (Fig. 4a). The lowering is probably due to lysosomal degradation of eEF2, because the effect could be blocked by the lysosome inhibitor CQ (Fig. 4a).

We investigated other potential changes of eEF2 in addition to the total level changes. Phosphorylation of eEF2 is known to interfere with its interaction with ribosomes, leading to reduced eEF2 translational functions[31]. Meanwhile, the level of phosphorylated eEF2 was reduced rather than increased in the HD cells or cells expressing exogenous eCAGr RNA (Fig. 4a), suggesting that eEF2 was not inactivated by enhanced phosphorylation. eEF2 clustering is also known to suppress its function[32], and thus we visualized eEF2 in the cells by immunofluorescence or fluorescent protein tagging. We observed significantly more eEF2

puncta in the HD ($STHdh^{Q7/Q111}$) but not WT ($STHdh^{Q7/Q7}$) cells (Extended Data Fig. 6a). Consistent with the observation in cells, we observed significantly increased eEF2 puncta in human patients (Fig. 4b) or brain slices from HD mice ($Hdh^{Q7/Q140}$) (Fig. 4c & Extended Data Fig. 6b), suggesting that eEF2 clustering could be a mechanism *via* which the eCAGr RNA influences translation elongation.

These eEF2 puncta in eCAGr RNA-expressing cells are likely to be solid-like condensates because they failed to recover after photo-bleaching (Extended Data Fig. 6c). The cells were treated with the lysosome inhibitor NH_4Cl to avoid the potential lysosomal clearance of the eEF2 puncta so that they could be visible. These eEF2 puncta colocalized with the lysosomes, confirming their lysosomal degradation (Extended Data Fig. 6d-e).

To confirm that the eEF2 puncta was caused by eCAGr RNA gelation, we utilized the optogenetic system (Fig. 3d) to induce the enhanced eCAGr RNA clustering and tracked eEF2 in live cells. Shining blue light on these cells led to drastic eEF2 puncta formation (Fig. 4d), confirming eEF2 clustering as a consequence of eCAGr RNA gelation. Taken together, the eCAGr RNA clustered and formed foci, which induced the puncta formation and degradation of eEF2.

To further elucidate the functional relevance of eEF2 changes in HD cells or cells expressing exogenous eCAGr RNA, we investigated eEF2's distribution in different fractions of the polysome profiling samples, and observed a significant reduction of eEF2 in the ribosomal subunit and monosome fractions (Extended Data Fig. 7a), suggesting that eEF2 dissociated with ribosomes in eCAGr RNA-expressing cells. Consistent with this, the colocalization between eEF2 and ribosomes was significantly reduced in the HD cells, whereas the eEF1-ribosome colocalization was not influenced (Extended Data Fig. 7b). In the *in vitro* translation system,

addition of the recombinant purified eEF2 protein rescued the translation deficits in the eCAGr RNA treated group (Fig. 4e), confirming that the functional loss of eEF2 could rescued simply by providing more eEF2.

Taken together, eEF2 clustering and its lysosomal degradation may mediate the eCAGr RNA's impact on global protein translation.

eCAGr RNA foci sequester eEF2

Why eCAGr RNA gelation may cause eEF2 clustering is intriguing. Our *in vitro* experiments showed that the recombinant purified eEF2 protein was able to form condensates in saline only with the presence of eCAGr RNA but not by itself (Extended Data Fig. 8), suggesting that the formation of eEF2 condensates could be facilitated by the eCAGr RNAs. The *in vitro* experiments demonstrated a possibility of eCAGr RNA gels sequestering and co-clustering with eEF2 to form condensates (Extended Data Fig. 8), although the *in vitro* condition could be very different from the condition inside the cells.

We then investigated this possibility by visualizing the eEF2 puncta and the eCAGr RNA foci in different systems. In WT cells ($STHdh^{Q7/Q7}$) co-expressing the eCAGr RNA (47×CAG-MS2) and GFP-fused eEF2, we observed strong colocalization between these two, with the RNA being detected by MS2CP-BFP (Fig. 5a). Such colocalization was not observed in the control groups expressing 12×CAG-MS2 with eEF2 or 47×CAG-MS2 with eEF1A (Fig. 5a). We observed the similar colocalization between GFP-fused eEF2 and endogenous eCAGr RNA foci in transfected HD ($STHdh^{Q7/Q111}$) but not WT ($STHdh^{Q7/Q7}$) cells (Fig. 5b). To further demonstrate this observation *in vivo* in an endogenous system, we visualized the endogenous mutant *HTT* mRNA foci containing the eCAGr by the RNAscope technology and the endogenous eEF2 protein by immunofluorescence in striatal brain slices from an HD knock-in

model $Hdh^{Q7/Q140}$ (Fig. 5c; the eEF2 antibody specificity was validated in Extended Data Fig. 9a). Most of the eCAGr RNA foci were surrounded and wrapped by the eEF2 puncta, which partially colocalized with them (Fig. 5c), suggesting that the eCAGr RNA foci may have sequestered eEF2. eEF2 was not detected in the cores of these foci, likely because these cores were inaccessible to the eEF2 antibody. Consistent with this, RNase treatment of these slices led to the increased and enhanced eEF2 puncta formation detected by immunofluorescence (Extended Data Fig. 9b).

Taken together, cytoplasmic eCAGr RNA may form solid-like foci similarly to its behaviour *in vitro*[1] (Fig. 1), and these foci may sequester eEF2 inside or around them, leading to the clustering of eEF2 and inhibition of eEF2 function in translation elongation (Fig. 5d).

Discussion

The discovery of LLPS and gelation of eCAGr RNA opens an exciting possibility that the eCAGr RNA may function independently of, or synergistically with expanded protein in repeat expansion disorders such as Huntington's disease[1,2], but there have been three missing parts in this beautiful scenario: the lack of "solid-like" properties of RNA foci in cells, the absence of cytoplasmic eCAGr foci, and a lack of functional studies. Our study resolved these mysteries: the cytoplasmic eCAGr foci do exist and exhibit the solid-like property that is consistent with their *in vitro* behaviour, but they are rapidly degraded by lysosomes (Fig. 1a-b, 1d). This demonstrates the role of lysosomal degradation in the clearance of eCAGr RNA foci, providing new entry points for intervention of repeat expansion disorders. The discovery also shed lights on the possible role of eCAGr RNA in neurodegeneration, consistent with recent discovery that the consecutive CAG-repeat number correlates with the age-of-onset of HD[33]. Potential eCAGr

RNA targeting strategies by gene therapy or small molecules could be desired for disease treatment[34,35].

The observation of solid-like cytoplasmic eCAGr RNA foci enables the study of functional impacts of RNA gelation, which was not observed previously[1]. Meanwhile, the functional study of RNA LLPS and gelation remains challenging due to a lack of approach to manipulate, especially to induce, the formation of RNA foci. We established a light-inducible eCAGr RNA foci formation system based on the eCAGr specific-binding peptide BIND[22] that successfully achieved this goal (Fig. 3d-e). This approach, along with previously published tools that disrupt eCAGr foci[1], allowed us to study the causal relationship between RNA gelation and its potential functional impacts.

The functional impacts turned out to be defects of global protein translation (Fig. 2). Recently, the change of global protein translation rates in repeat expansion disorders such as HD has been studied but remained controversial, with both upregulation and downregulation of global translation rates reported in different studies[12-17]. The reported mechanisms have also been fundamentally different, and none of them involves eCAGr RNA. Thus, the global protein translation in repeat expansion disorders is likely influenced by multiple mechanisms, and the ultimate outcome could be variable depending on the experimental models, conditions, and measurement approaches. For example, the SUnSET assay utilized in recent studies detects the overall abundance of puromycin-labeled translating peptides at a certain time point[14,25], and thus reflects the number of working ribosomes rather than the movement speed of these ribosomes on mRNAs. Thus, the elongation defects may not be reflected by the SUnSET signals.

To establish the causal relationship between eCAGr RNAs and global protein translation, our data illustrate that the addition of eCAGr RNA for minutes were able to reduce the reporter

protein translation in the *in vitro* translation system (Fig. 2g). In addition, we manipulated the eCAGr RNA foci in both directions and observed subsequent changes in the protein translation rates (Fig. 3a-b & f), establishing a novel causal relationship between RNA gelation and protein translation. Meanwhile, we could not exclude the possibility that other cellular mechanisms downstream of the pathogenic proteins may also influence protein translation.

Our study reveals that the RNA gelation may sequester the key elongation factor eEF2 to slow down translation elongation (Fig. 4, Extended Data Fig. 6). Global translation regulation by eEF2 is usually mediated by its phosphorylation[31,36]. Recently studies suggest that its misfolding and aggregation during its own synthesis are also capable of influencing its function[32]. Our study suggests another novel mechanism of eEF2-mediated translation regulation: its sequestration by RNA LLPS and gelation. The significance of this cellular mechanism remains to be further explored in CAG expansion disorders and possibly in other RNA LLPS related pathological or physiological conditions.

In summary, our discoveries revealed the novel cytoplasmic RNA gelation inside the cells and revealed its functional impact: suppressing global protein translation elongation *via* sequestering eEF2. The contribution of RNA gelation to neurodegeneration remains to be studied. Interestingly, the rate of protein elongation was estimated to decline up to 80% during ageing[37]. Consistent with this, up to a 2-fold decrease in elongation rate in aged rat tissues relative to young counterparts was reported[38,39]. The decreased protein translation could be a compensatory mechanism to prevent cell death during ageing[40], but this might be exacerbated in CAG repeat expansion disorders, leading to loss of critical neuronal functions or neurodegeneration. The potential synergic effects between ageing and eCAGr RNA-induced lowering of global protein translation remain to be further explored.

References

1 Jain, A. & Vale, R. D. RNA phase transitions in repeat expansion disorders. *Nature* **546**, 243-247, doi:10.1038/nature22386 (2017).

2 Sanders, D. W. & Brangwynne, C. P. Neurodegenerative disease: RNA repeats put a freeze on cells. *Nature* **546**, 215-216, doi:10.1038/nature22503 (2017).

3 La Spada, A. R. & Taylor, J. P. Repeat expansion disease: progress and puzzles in disease pathogenesis. *Nat Rev Genet* **11**, 247-258, doi:10.1038/nrg2748 (2010).

4 Gardiner, S. L. *et al.* Prevalence of Carriers of Intermediate and Pathological Polyglutamine Disease-Associated Alleles Among Large Population-Based Cohorts. *JAMA Neurol* **76**, 650-656, doi:10.1001/jamaneurol.2019.0423 (2019).

5 Van Treeck, B. & Parker, R. Emerging Roles for Intermolecular RNA-RNA Interactions in RNP Assemblies. *Cell* **174**, 791-802, doi:10.1016/j.cell.2018.07.023 (2018).

6 Lamark, T. & Johansen, T. Aggrephagy: selective disposal of protein aggregates by macroautophagy. *Int J Cell Biol* **2012**, 736905, doi:10.1155/2012/736905 (2012).

7 Fujiwara, Y., Wada, K. & Kabuta, T. Lysosomal degradation of intracellular nucleic acids-multiple autophagic pathways. *J Biochem* **161**, 145-154, doi:10.1093/jb/mvw085 (2017).

8 Fujiwara, Y. *et al.* Discovery of a novel type of autophagy targeting RNA. *Autophagy* **9**, 403-409, doi:10.4161/auto.23002 (2013).

9 Trettel, F. *et al.* Dominant phenotypes produced by the HD mutation in STHdh(Q111) striatal cells. *Hum Mol Genet* **9**, 2799-2809 (2000).

10 Mizushima, N. *et al.* A protein conjugation system essential for autophagy. *Nature* **395**, 395-398, doi:10.1038/26506 (1998).

11 Mizushima, N. *et al.* Dissection of autophagosome formation using Apg5-deficient mouse embryonic stem cells. *The Journal of cell biology* **152**, 657-668, doi:10.1083/jcb.152.4.657 (2001).

12 Joag, H. *et al.* A role of cellular translation regulation associated with toxic Huntingtin protein. *Cell Mol Life Sci* **77**, 3657-3670, doi:10.1007/s00018-019-03392-y (2020).

13 Athar, Y. M. & Joseph, S. The Human Fragile X Mental Retardation Protein Inhibits the Elongation Step of Translation through Its RGG and C-Terminal Domains. *Biochemistry* **59**, 3813-3822, doi:10.1021/acs.biochem.0c00534 (2020).

14 Creus-Muncunill, J. *et al.* Increased translation as a novel pathogenic mechanism in Huntington's disease. *Brain* **142**, 3158-3175, doi:10.1093/brain/awz230 (2019).

15 Brouillet, E. & Merienne, K. What is gained or 'lost in translation' in Huntington's disease. *Brain* **142**, 2900-2902, doi:10.1093/brain/awz274 (2019).

16 Jacquemont, S. *et al.* Protein synthesis levels are increased in a subset of individuals with fragile X syndrome. *Hum Mol Genet* **27**, 2039-2051, doi:10.1093/hmg/ddy099 (2018).

17 Eshraghi, M. *et al.* Mutant Huntingtin stalls ribosomes and represses protein synthesis in a cellular model of Huntington disease. *Nat Commun* **12**, 1461, doi:10.1038/s41467-021-21637-y (2021).

18 McGuire, A. M., Matsuo, H. & Wagner, G. Internal and overall motions of the translation factor eIF4E: cap binding and insertion in a CHAPS detergent micelle. *J Biomol NMR* **12**, 73-88, doi:10.1023/a:1008214128792 (1998).

19 Ma, T. *et al.* Suppression of eIF2alpha kinases alleviates Alzheimer's disease-related plasticity and memory deficits. *Nat Neurosci* **16**, 1299-1305, doi:10.1038/nn.3486 (2013).

20 Moreno, J. A. *et al.* Sustained translational repression by eIF2alpha-P mediates prion neurodegeneration. *Nature* **485**, 507-511, doi:10.1038/nature11058 (2012).

21 Shieh, S. Y. & Bonini, N. M. Genes and pathways affected by CAG-repeat RNA-based toxicity in Drosophila. *Hum Mol Genet* **20**, 4810-4821, doi:10.1093/hmg/ddr420 (2011).

22 Zhang, Q. *et al.* A peptidylic inhibitor for neutralizing expanded CAG RNA-induced nucleolar stress in polyglutamine diseases. *RNA* **24**, 486-498, doi:10.1261/rna.062703.117 (2018).

23 Bugaj, L. J., Choksi, A. T., Mesuda, C. K., Kane, R. S. & Schaffer, D. V. Optogenetic protein clustering and signaling activation in mammalian cells. *Nat Methods* **10**, 249-252, doi:10.1038/nmeth.2360 (2013).

24 Sinturel, F. *et al.* Diurnal Oscillations in Liver Mass and Cell Size Accompany Ribosome Assembly Cycles. *Cell* **169**, 651-663 e614, doi:10.1016/j.cell.2017.04.015 (2017).

25 Schmidt, E. K., Clavarino, G., Ceppi, M. & Pierre, P. SUnSET, a nonradioactive method to monitor protein synthesis. *Nat Methods* **6**, 275-277, doi:10.1038/nmeth.1314 (2009).

26 Deng, Z. *et al.* Myostatin inhibits eEF2K-eEF2 by regulating AMPK to suppress protein synthesis. *Biochem Biophys Res Commun* **494**, 278-284, doi:10.1016/j.bbrc.2017.10.040 (2017).

27 Kasari, V., Margus, T., Atkinson, G. C., Johansson, M. J. O. & Hauryliuk, V. Ribosome profiling analysis of eEF3-depleted Saccharomyces cerevisiae. *Scientific reports* **9**, 3037, doi:10.1038/s41598-019-39403-y (2019).

28 Arguello, R. J. *et al.* SunRiSE - measuring translation elongation at single-cell resolution by means of flow cytometry. *J Cell Sci* **131**, doi:10.1242/jcs.214346 (2018).

29 Darnell, J. C. *et al.* FMRP stalls ribosomal translocation on mRNAs linked to synaptic function and autism. *Cell* **146**, 247-261, doi:10.1016/j.cell.2011.06.013 (2011).

30 Dever, T. E., Dinman, J. D. & Green, R. Translation Elongation and Recoding in Eukaryotes. *Cold Spring Harb Perspect Biol* **10**, doi:10.1101/cshperspect.a032649 (2018).

31 Carlberg, U., Nilsson, A. & Nygard, O. Functional properties of phosphorylated elongation factor 2. *Eur J Biochem* **191**, 639-645, doi:10.1111/j.1432-1033.1990.tb19169.x (1990).

32 Monkemeyer, L. *et al.* Chaperone Function of Hgh1 in the Biogenesis of Eukaryotic Elongation Factor 2. *Molecular cell* **74**, 88-100 e109, doi:10.1016/j.molcel.2019.01.034 (2019).

33 Consortium, G. M. o. H. s. D. CAG Repeat Not Polyglutamine Length Determines Timing of Huntington's Disease Onset. *Cell* **178**, 887-900 e814, doi:10.1016/j.cell.2019.06.036 (2019).

34 Tabrizi, S. J. *et al.* Targeting Huntingtin Expression in Patients with Huntington's Disease. *N Engl J Med* **380**, 2307-2316, doi:10.1056/NEJMoa1900907 (2019).

35 Angelbello, A. J. *et al.* A Small Molecule that Binds an RNA Repeat Expansion Stimulates Its Decay via the Exosome Complex. *Cell Chem Biol* **28**, 34-45 e36, doi:10.1016/j.chembiol.2020.10.007 (2021).

36 Kaul, G., Pattan, G. & Rafeequi, T. Eukaryotic elongation factor-2 (eEF2): its regulation and peptide chain elongation. *Cell Biochem Funct* **29**, 227-234, doi:10.1002/cbf.1740 (2011).

37 Rattan, S. I. Synthesis, modifications, and turnover of proteins during aging. *Experimental gerontology* **31**, 33-47, doi:10.1016/0531-5565(95)02022-5 (1996).

38 Merry, B. J. & Holehan, A. M. Effect of age and restricted feeding on polypeptide chain assembly kinetics in liver protein synthesis in vivo. *Mech Ageing Dev* **58**, 139-150, doi:10.1016/0047-6374(91)90088-h (1991).

39 Khasigov, P. Z. & Nikolaev, A. Age-related changes in the rates of polypeptide chain elongation. *Biochem Int* **15**, 1171-1178 (1987).

40 Steffen, K. K. & Dillin, A. A Ribosomal Perspective on Proteostasis and Aging. *Cell Metab* **23**, 1004-1012, doi:10.1016/j.cmet.2016.05.013 (2016).

Main figures and legends:

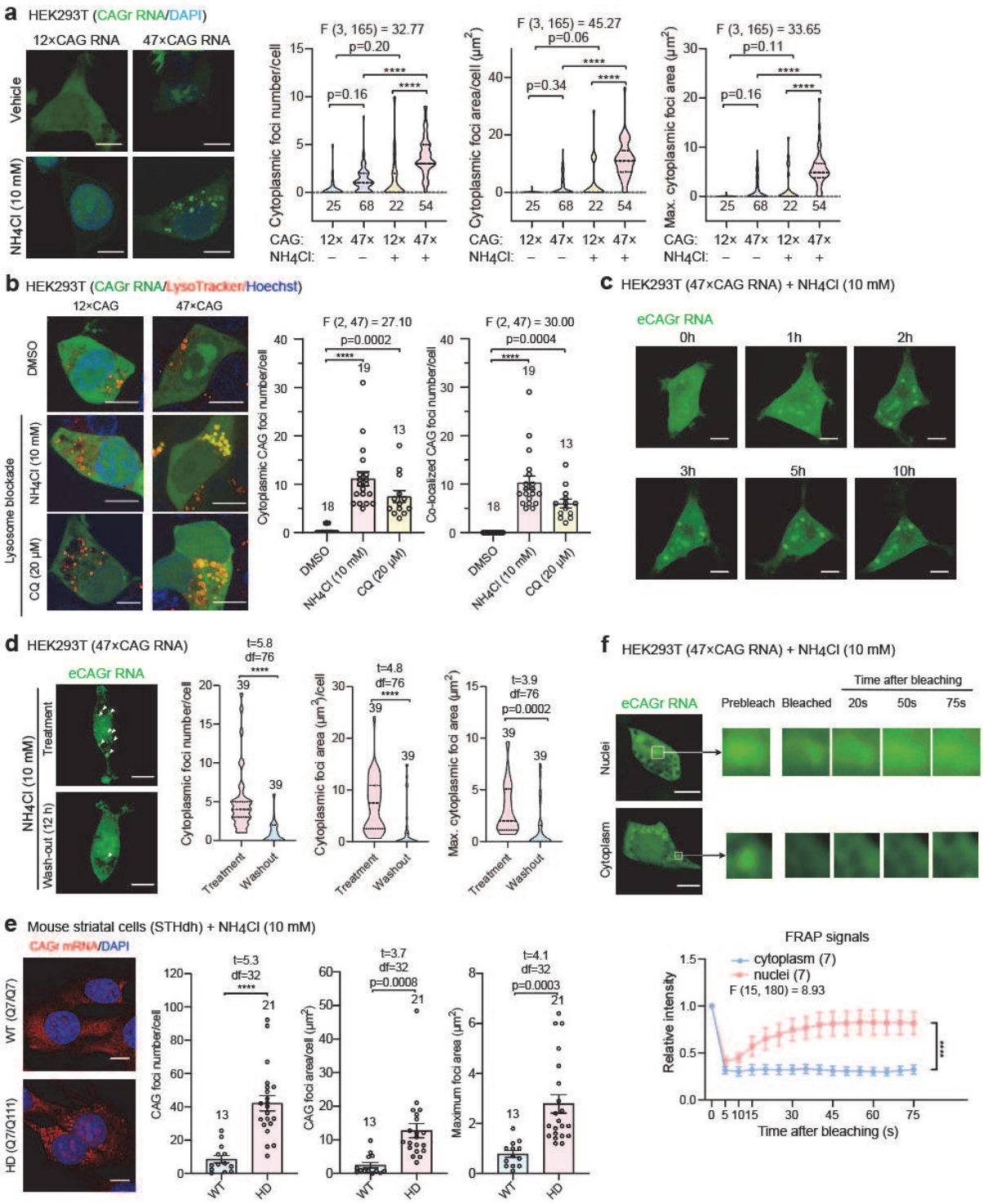

Fig. 1: The eCAGr RNA forms cytoplasmic gel-like condensates that are degraded by the lysosomes. a. Representative images and quantifications of eCAGr RNA condensates (foci) in

transfected HEK293T cells expressing the indicated RNA together with MS2CP-YFP as the foci detector. **b.** Representative images and quantifications of eCAGr RNA foci and the lysosomes in HEK293T cells treated with the indicated lysosome inhibitors (NH_4Cl and CQ). **c-d.** Snap-shots and quantifications of the representative live cell imaging showing that the eCAGr RNA foci appeared in the cytoplasm after adding the lysosome inhibitor NH_4Cl but not the vehicle (culture medium) control (**c**), and disappeared after washing out NH_4Cl (**d**). eCAGr RNA foci are indicated by white arrows (**d**). **e.** Representative images and quantifications of RNA foci by RNA FISH in STHdh cells treated with the indicated lysosome inhibitors versus the control. **f.** Representative images and quantifications of the FRAP experiments for the eCAGr foci in the nuclei versus cytoplasm. Data are mean ± s.e.m.; analyzed by one-way ANOVA with multiple comparisons (**a**, **b**), or unpaired two-tailed t tests (**d**, **e**), or two-way ANOVA (**f**). The numbers of cells are shown in each plot. ****: $p < 0.0001$. Scale bars, 10 μm (**a-f**).

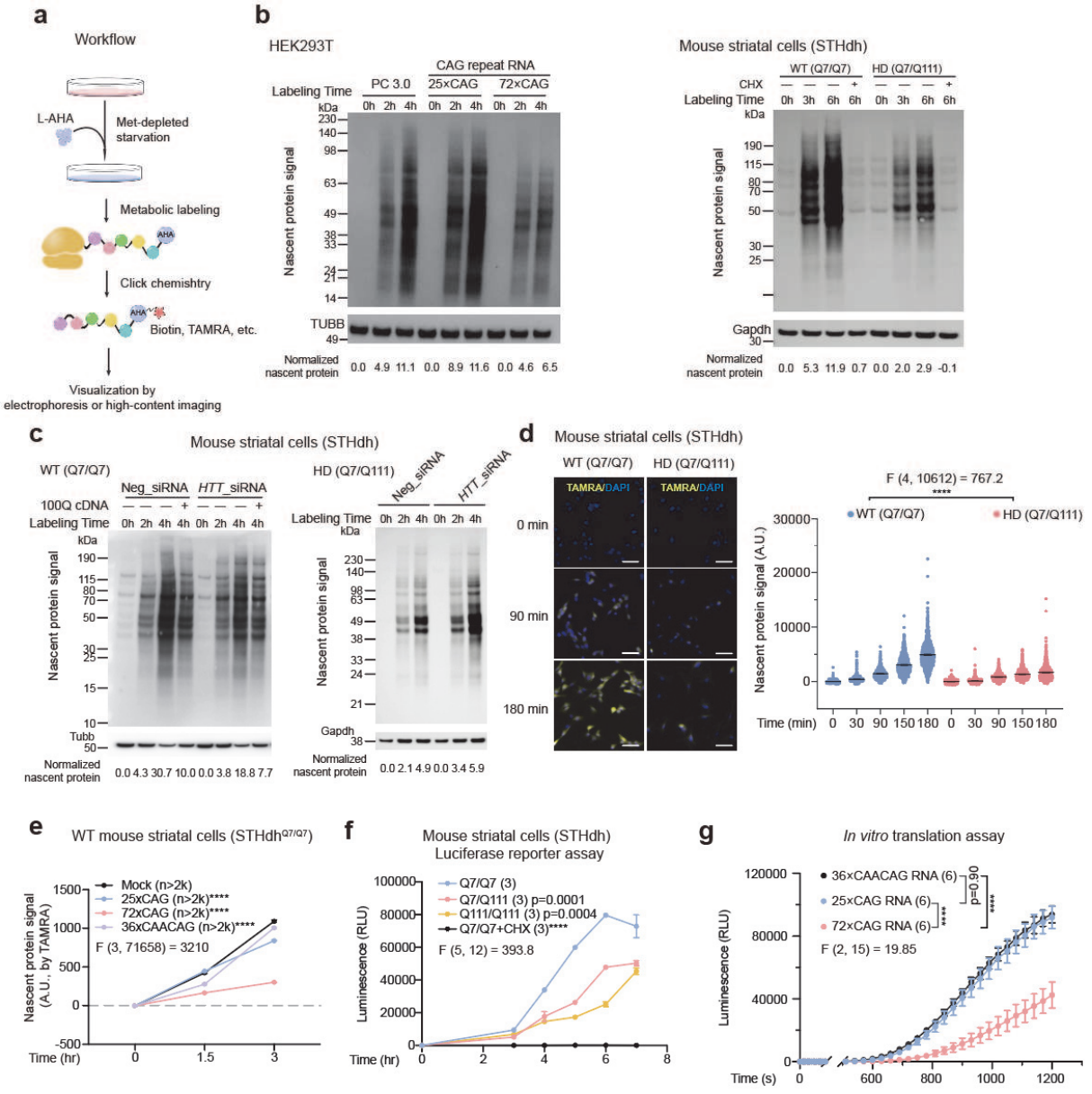

Fig. 2: The eCAGr RNA gelation inhibits global protein translation. a. Schematic showing the metabolic nascent protein labeling assays with the methionine analog L-AHA. **b.** Representative western-blots (from 5) of nascent proteins at indicated time points after metabolic labeling in HEK293T transfected with the indicated plasmids for 24 hours (*left*) or HD mouse striatal cells ($STHdh^{Q7/Q111}$) expressing endogenous mutant *HTT* mRNA containing eCAGr, versus the WT cells ($STHdh^{Q7/Q7}$) expressing no eCAGr RNAs (*right*). The nascent proteins were labeled for different length of time by the methionine analog L-AHA, which was then conjugated with biotin by Click-chemistry for detection using streptavidin-HRP. The protein translation

inhibitor cycloheximide (CHX)-treated groups were tested in the STHdh cells to ensure the specificity of the signals. **c.** Similar to **a**, but in STHdh cells transfected with the indicated siRNA or cDNA (100Q: full-length *HTT* cDNA containing 100×CAG). **d.** Representative high-content imaging and quantifications of nascent proteins in the STHdh$^{Q7/Q111}$ versus STHdh$^{Q7/Q7}$ cells at indicated time points after metabolic labeling. **e.** Quantifications of high-content images of nascent proteins in STHdh$^{Q7/Q7}$ cells transfected with the indicated plasmids at indicated time points after metabolic labeling. The nascent proteins were labeled for different length of time by the methionine analog L-AHA, which was then conjugated with TAMRA by Click-chemistry for visualization at the single cell level after fixing the cells. **f.** The luciferase reporter assay measuring the protein translation rate in WT (STHdh$^{Q7/Q7}$) or HD (STHdh$^{Q7/Q111}$ and STHdh$^{Q111/Q111}$) mouse striatal cells upon transfection of the reporter mRNA. **g.** The luciferase reporter assay measuring the protein translation rate in the *in vitro* translation system (using rabbit reticulocyte cell extracts) pre-treated with the indicated RNAs for 5 minutes. Data are mean ± s.e.m.; analyzed by two-way ANOVA with multiple comparisons (**d-g**). The numbers of cells (**d-e**) or the numbers of independently repeated wells (**f-g**) are shown in each plot. ****: p <0.0001. Scale bars, 20 μm (**d**).

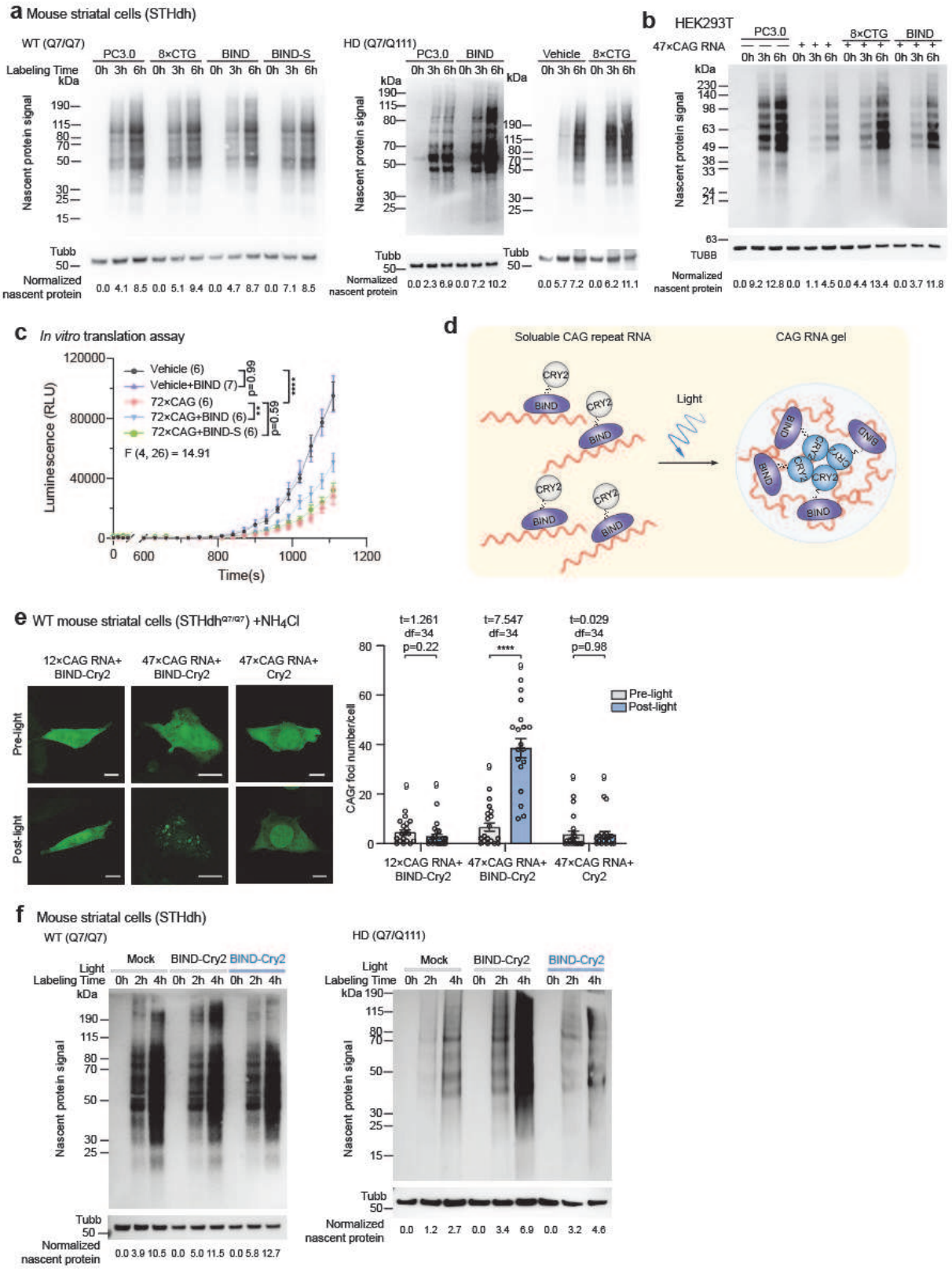

Fig. 3: The RNA gelation is likely the major cause of global protein translation inhibition.

a. Representative western-blots (from 5) of nascent proteins at indicated time points after metabolic labeling in WT (Q7/Q7) or HD (Q7/Q111) mouse striatal cells transfected with the indicated oligonucleotides (8×CTG) or plasmids (empty pcDNA 3.0 vector (PC3.0) or the one expressing eCAGr RNA-binding peptide (BIND) versus the control (BIND-S)). **b.** Similar to a, but in HEK293T cells. **c.** Luciferase reporter assay measuring the protein translation rate of the *in vitro* translation system pre-treated with the indicated synthetic peptides and/or *in vitro* transcribed RNAs for 5 minutes. **d.** Schematic showing the optogenetic system that manipulates eCAGr RNA gelation: the blue light is used to trigger or enhance the assembly of eCAGr RNA condensates. **e.** Representative images and quantifications showing the enhanced clustering of eCAGr RNA upon the blue light stimulation in NH_4Cl-treated WT cells ($STHdh^{Q7/Q7}$) transfected with the indicated plasmids. **f.** Similar to **a**, but in WT or HD mouse striatal cells transfected with the indicated plasmids with (blue bars on top of the gel) or without (white bars on top of the gel) the blue light exposure. Enhancement in eCAGr RNA condensate formation disabled the rescue effect of BIND on protein translation which was suppressed by the eCAGr RNA gelation. Data are mean ± s.e.m.; analyzed by two-way ANOVA with multiple comparisons (**c**) or two tailed unpaired t tests (**e**). The numbers of independently repeated wells (**c**) or the numbers of cells (**e**) are shown in each plot. ****: $p < 0.0001$. Scale bars, 10 μm (**e**).

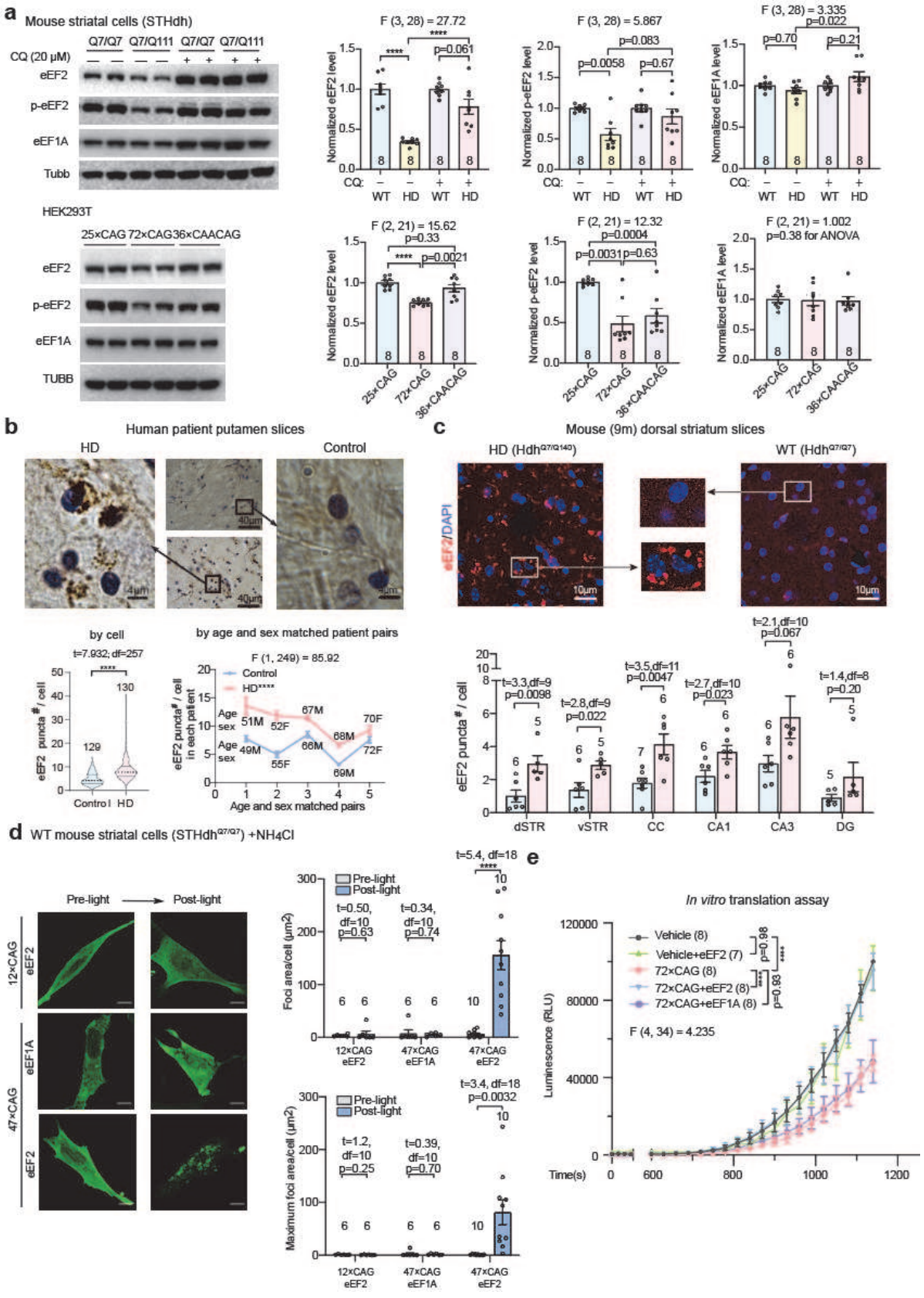
a
Mouse striatal cells (STHdh)
Q7/Q7 Q7/Q111 Q7/Q7 Q7/Q111
CQ (20 μM)
eEF2
p-eEF2
eEF1A
Tubb
HEK293T
25×CAG 72×CAG 36×CAACAG
TUBB
F (3, 28) = 27.72
p=0.061
Normalized eEF2 level
F (3, 28) = 5.867
p=0.083
p=0.0058
p=0.67
Normalized p-eEF2 level
F (3, 28) = 3.335
p=0.022
p=0.70
p=0.21
Normalized eEF1A level
WT HD WT HD
F (2, 21) = 15.62
p=0.33
p=0.0021
F (2, 21) = 12.32
p=0.0004
p=0.0031 p=0.63
F (2, 21) = 1.002
p=0.38 for ANOVA
25×CAG 72×CAG 36×CAACAG
b
Human patient putamen slices
HD
Control
by cell
t=7.932; df=257
eEF2 puncta # / cell
Control HD
by age and sex matched patient pairs
F (1, 249) = 85.92
Control
HD****
Age sex
51M 52F 67M 70F
49M 55F 66M 68M 72F 69M
eEF2 puncta # in each patient
Age and sex matched pairs
c
Mouse (9m) dorsal striatum slices
HD (Hdh Q7/Q143)
WT (Hdh Q7/Q7)
eEF2/DAPI
10μm
t=3.3,df=9 p=0.0098
t=2.8,df=9 p=0.022
t=3.5,df=11 p=0.0047
t=2.7,df=10 p=0.023
t=2.1,df=10 p=0.067
t=1.4,df=8 p=0.20
eEF2 puncta # / cell
dSTR vSTR CC CA1 CA3 DG
d
WT mouse striatal cells (STHdh Q7/Q7) +NH4Cl
Pre-light Post-light
12×CAG eEF2
47×CAG eEF1A
47×CAG eEF2
t=5.4, df=18
t=0.50, df=10 p=0.63
t=0.34, df=10 p=0.74
Foci area/cell (μm2)
12×CAG eEF2
47×CAG eEF1A
47×CAG eEF2
t=3.4, df=18 p=0.0032
t=1.2, df=10 p=0.25
t=0.39, df=10 p=0.70
Maximum foci area/cell (μm2)
e
In vitro translation assay
Vehicle (8)
Vehicle+eEF2 (7)
72×CAG (8)
72×CAG+eEF2 (8)
72×CAG+eEF1A (8)
p=0.98
p=0.93
F (4, 34) = 4.235
Luminescence (RLU)
Time(s)

Fig. 4: eCAGr RNA foci induced eEF2 clustering and degradation. a. Representative western-blots and quantifications of eEF2, phospho-eEF2 and eEF1A levels in the indicated cells treated/transfected with the indicated compounds or plasmids, respectively. CQ: chloroquine. **b.** Representative immunohistochemistry images (from > 25 images per patient) and quantifications (in total or within the age matched pairs) showing the endogenous eEF2 puncta in HD versus WT human putamen slices. **c.** Representative immunofluorescence images of dorsal striatum and quantifications of diverse brain sections showing the eEF2 puncta in HD ($Hdh^{Q7/Q140}$) versus WT ($Hdh^{Q7/Q7}$) mouse slices (n indicates the number of mice). **d.** Snapshots of representative live cell imaging and quantifications of exogenously expressed eEF2-sfGFP or eEF1A-sfGFP puncta in NH_4Cl-treated WT or HD mouse striatal cells upon blue light exposure. Scale bars: 10 μm. **e.** Luciferase reporter assay measuring the translation rate in the *in vitro* translation system pre-treated with the indicated recombinant purified proteins and/or *in vitro* transcribed RNAs for 5 minutes. Data are mean ± s.e.m.; analyzed by one-way ANOVA with multiple comparisons (**a**), two-way ANOVA (**b),** two-way ANOVA with multiple comparisons (**e**), or two-tailed unpaired t tests (**b**-**d**). The numbers of independently repeated samples (**a**), images **(b)**, mice (**c**), wells (**e**), or the numbers of cells (**d**) are shown in each plot. ****: $p < 0.0001$.

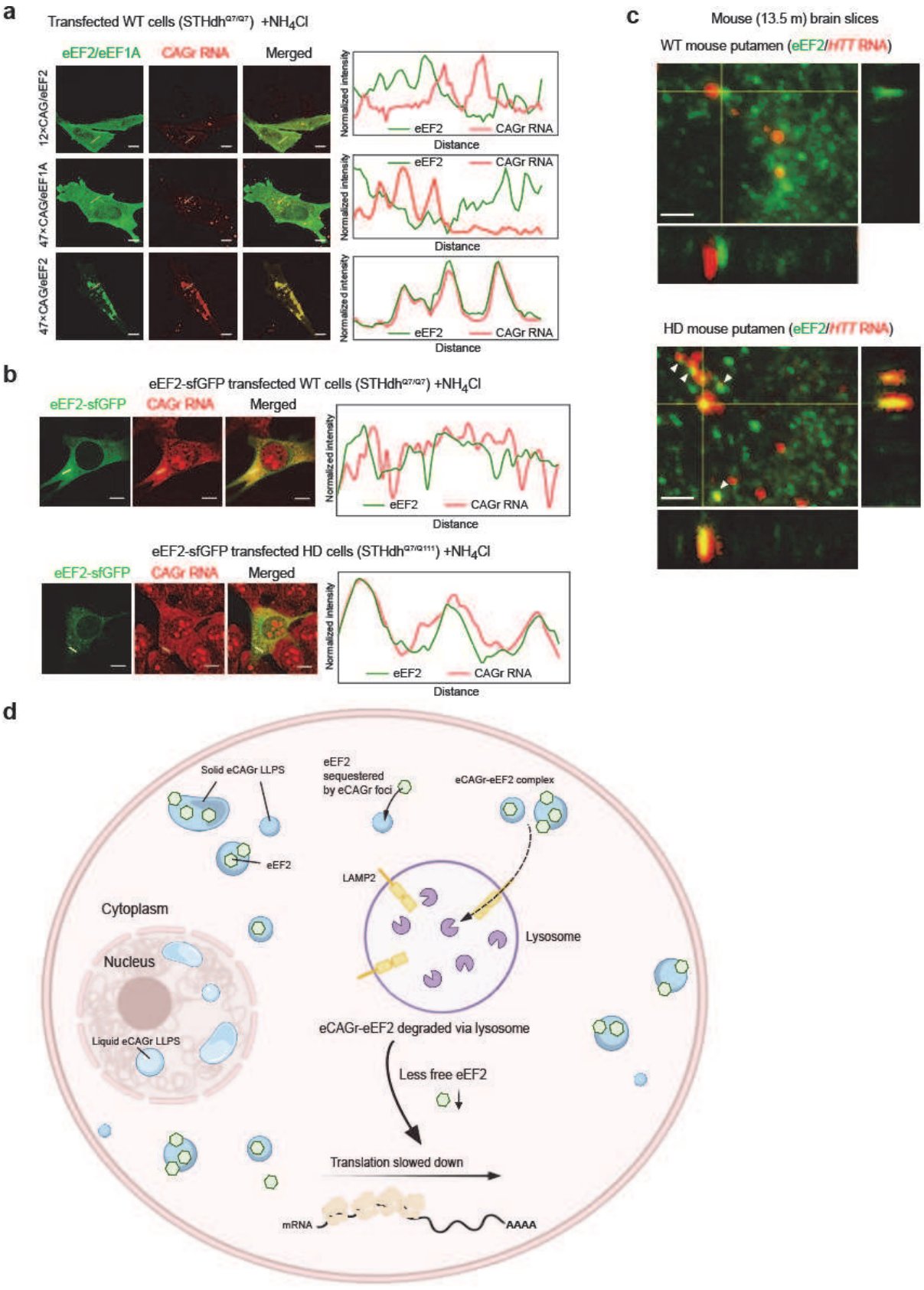
a
Transfected WT cells (STHdh$^{Q7/Q7}$) +NH_4Cl
eEF2/eEF1A
CAGr RNA
Merged
12×CAG/eEF2
47×CAG/eEF1A
47×CAG/eEF2
Normalized intensity
eEF2
CAGr RNA
Distance
b
eEF2-sfGFP transfected WT cells (STHdh$^{Q7/Q7}$) +NH_4Cl
eEF2-sfGFP
CAGr RNA
Merged
eEF2-sfGFP transfected HD cells (STHdh$^{Q7/Q111}$) +NH_4Cl
c
Mouse (13.5 m) brain slices
WT mouse putamen (eEF2/HTT RNA)
HD mouse putamen (eEF2/HTT RNA)
d
Solid eCAGr LLPS
eEF2
eEF2 sequestered by eCAGr foci
eCAGr-eEF2 complex
LAMP2
Lysosome
Cytoplasm
Nucleus
Liquid eCAGr LLPS
eCAGr-eEF2 degraded via lysosome
Less free eEF2
Translation slowed down
mRNA
AAAA

Fig. 5: eCAGr RNA foci sequestered eEF2. a. Representative fluorescent images (from > 6) of NH_4Cl-treated WT mouse striatal cells co-transfected with eCAGr RNA (47×CAG-MS2), MS2CP-BFP, eEF2-sfGFP or eEF1A-sfGFP. The 12×CAG-MS2, MS2CP-BFP and eEF2-sfGFP were also transfected into the cells for the control purpose. Colocalization patterns between eCAGr RNA and eEF2/eEF1A at the beige lines are plotted. Scale bars, 10 μm. **b.** Representative RNAScope/ immunofluorescence images (from 3 mice in each group) of the CAGr RNA (detected by FISH) and eEF2 in NH_4Cl-treated WT/HD mouse striatal cells transfected with GFP-eEF2. Colocalization patterns between CAGr RNA and eEF2 at the beige lines are visualized. Scale bars, 10 μm. **c.** Representative images (from 3 mice in each group) showing the colocalization between endogenous eCAGr RNA foci and eEF2 puncta in HD mouse brain slices versus the WT brain slices. Colocalizations of eEF2 and *HTT* RNA are indicated by white arrows. Scale bars, 2 μm. **d.** Schematic showing that the eCAGr RNA foci sequesters eEF2 and are subject to lysosomal clearance *via* LAMP2, leading to global protein translation deficits.

Supplementary Materials for

The Gelation of CAG Repeat Expansion RNAs Suppresses Global Protein Translation

Materials and Methods

Mammalian cell lines

The mouse striatal cells, STHdh (obtained from Coriell Cell Repositories), were cultured at 33 °C with 5% CO_2 in DMEM (ThermoFisher Scientific, cat. no. 11965) with 10% (vol/vol) FBS (ThermoFisher Scientific, cat. no. 10082). The HEK293T cells (from ATCC) and MEFs (mouse embryo fibroblasts) were cultured in the same medium but at 37 °C with 5% CO_2. The Atg5 knockout MEFs and the wild-type control cells[1] were kindly provided by Dr. Mizushima. All the cells were tested for mycoplasma contamination every two months.

Plasmids

All cloning and amplification were performed in TransStbl3 Chemically Competent Cell (Transgen, cat. no. CD521-01). To generate the pHR-TAT-BIND-mCherry-Cry2oligo plasmid, the pHR-mCh-Cry2olig plasmid[2] was purchased (Addgene, cat. no.101222). The double strand oligonucleotides TAT-BIND-myc was annealed from primers TAT-BIND-myc-F and TAT-BIND-myc-R (sequences provided in Supplementary Table 1)[3], and cloned into pHR-mCh-Cry2olig using the Seamless Cloning Kit (Tiangen, cat. no. VI201). The 47×CAG (cat.no. 99148), rtTA (cat.no. 66810), MCP-YFP (cat.no. 99151) and pLAMP1-mCherry (cat. no. 45147) plasmids were also purchased from Addgene. The 12×CAG plasmid was generated from the 47×CAG through the transformation and colony selection. The 72×CAG (with 5' 6×stop codons), 25×CAG (with 5' 6×stop codons), 72×Cys, 72×Ser or 72×Glu (the latter three all with 5' ATG and Kozak sequences) are custom synthesized by Genescript (sequences provided in Supplementary Table 1) and sequence validated. For recombinant protein purification and

expression in mammalian cells, the human *EEF2* (GenBank: NM_001961.4) or *EEF1A* gene (GenBank: NM_001402.6) was cloned into a modified pTT vector with C-terminal sfGFP and His_8 tag, and sequence validated. The plasmids were kind gifts from Dr. Yu Ding (*EEF2*) and Dr. Jinzhong Lin (*EEF1A*), respectively.

Mouse models

The generation and characterization of the Hdh^{140Q} knock-in mice have been previously described[4]. The original mice utilized to start to colony were kind gifts from Dr. Marian Difiglia's group. Mice were group-housed (up to 5 adult mice per cage) in individually vented cages with a 12-hour light/dark cycle. The mouse experiments were carried out following the general guidelines published by the Association for Assessment and Accreditation of Laboratory Animal Care. The Animal Care and Use Committee approved the protocol used in animal experiments (Approval #20170223-005).

Immunofluorescence

For brain section staining, mice were anesthetized with sodium pentobarbital. Transcardial perfusion was then performed with 0.9% saline (40 mL) and subsequently 4% paraformaldehyde (PFA) in 0.9% saline (40 mL). Brains were post-fixed with 4% PFA in 0.9% saline overnight at 4°C. The coronal sections (20 μm) were then cut using a cryostat slicer (Leica, CM1950) for immunofluorescence. For culture staining, the cells were fixed in 4% PFA for 15 min at room temperature. Sections or cells were then transferred into blocking solution (5% bovine serum albumin, 0.5% Triton X-100, and 0.05% sodium azide in phosphate-buffered saline (PBS)) in a multi-well plate, placed on a shaker, and shaken gently at room temperature for 1.5–2 h, followed by overnight incubation (4 °C) with the primary antibodies. After washing with PBST (0.1% Triton X-100 in PBS) for 10 min thrice, the sections or cells were incubated with the secondary antibodies for 1–2h at room temperature. Sections or cells were then mounted with Fluoromount-G containing DAPI (Southern Biotech, cat. no. 0100-20). Fluorescence images were captured with a Zeiss LSM 880 or an Olympus Fluoview FV3000 confocal microscope. eEF2 puncta were analyzed with FIJI using a fluorescence-intensity and size-based threshold.

Live cell imaging

35 mm 4-chamber or ordinary glass-bottom dishes (Cellvis, cat. no. D35C4-20-1-N) were coated with 2% gelatin for 2 h at room temperature and dried for 1 h. Cells were plated in the dish before transient transfection with about 50% confluency. phR-tdMCP-YFP (Addgene, cat.

no.99151), pHR-Tre3G-12×CAG-12×MS2 or pHR-Tre3G-47×CAG-12×MS2 (Jain, 2017), rtTA (Addgene, cat. no.66810) (mass ratio of 2:2:1) were co-transfected into the cell using lipofectamine 3000 (ThermoFisher Scientific, cat. no. L3000) as instructed. Cells were added with 1000 ng/mL doxycycline to induce the CAG RNA expression for 24 h, treated with the lysosomal inhibitor as indicated, and subsequently imaged by Dragonfly 200 (Andor).

Lysotracker colocalization assay

Cells were seeded in a 4-chamber 35 mm glass bottom dish, after transient transfection of indicated plasmids, siRNAs and/or compounds. LysoTracker™ Red DND-99 (ThermoFisher Scientific, cat. No. L7528) were diluted in culture medium with the final concentration of 500 nM. Cells were incubated with LysoTracker for 1h and then washed once after removing the medium. Subsequently, the labeled cells were imaged by Dragonfly 200.

Wash-out experiment

After transfection with phR-tdMCP-YFP, pHR-Tre3G-47×CAG-12×MS2, rtTA (mass ratio of 2:2:1) with doxycycline and NH_4Cl treatment for 24 h, the cells were washed once with DMEM and induced without NH_4Cl for 12 h. After induction, the cells were fixed, stained with DAPI, and imaged by Dragonfly 200.

Cell viability assay

Cell viability was measured using CellTiter-GLO Luminescent Cell Viability kit (Promega, cat. no. G7570), according to the manufacturer's instructions. Briefly, cells were transfected and then plated in 96-well plates (Nunc, cat. no. 167008) at a density of 20000/well and incubated at 33°C overnight. In the following day, the plates were equilibrated at room temperature for approximately 30 min, and then 100 μL CellTiter-GLO Reagent was added to each well. Cell lysis was induced by mixing 2 min. Before recording luminescence with a microplate luminometer (PerkinElmer Envision 2104), the plate was dark adapted for 10 min at room temperature to stabilize the luminescence signal.

Photoactivated assembly of eCAGr RNA condensates

Glass-bottom dishes were coated with 2% gelatin for 2 h at room temperature and dried for 1 h. Cells were seeded onto the coated dishes right before transient transfection with about 30% confluency. phR-tdMCP-YFP, pHR-Tre3G-12×CAG-12×MS2 or pHR-Tre3G-47×CAG-12×MS2, rtTA, together with pHR-TAT-BIND-mCh-Cry2oligo or pHR-mCh-Cry2oligo (mass ratio of 2:2:1:5) were co-transfected into the cell using Lipofectamine 3000 as instructed, except

that the total plasmid amount used was doubled. To maintain similar expression level of TAT-BIND-mCh-Cry2oligo and mCh-Cry2oligo, two third of mCh-Cry2oligo used was replaced by tantamount mass of pcDNA3.0 RNA expression and lysosomal inhibition were induced by adding 1,000 ng/mL doxycycline and 10 mM NH_4Cl 24 h after transfection. 48 h after transfection, cells were imaged by a spinning disk confocal microscope IX83 (OLYMPUS) with the Dragonfly 200, with the 60× numerical aperture oil immersion. Cells were carefully protected from any light exposure except those from the microscope. After pre-light imaging, cells were treated with blue light from homemade blue-light array in a 33 ℃ incubator for 2 h. Right after light treatment, cells were fixed by 4% PFA at room temperature for 15 min and washed with PBS. Then cells were imaged again with the same conditions as pre-light imaging. During all the imaging process, cells were kept in a 33 °C live-cell imaging chamber supplemented with 5% CO_2.

Fluorescence Recovery After Photobleaching (FRAP) assay

For CAG RNA: Photoactivated assembly of eCAGr was induced as described above. Subsequently, the light-induced intracellular foci were bleached by 405 nm laser, and the fluorescence recovery was then monitored. During the imaging of fluorescence recovery in different cells, the cells were treated with 488 nm blue light from LED light with 50% intensity to maintain the photoactivated assembly. Fluorescence intensity was quantified using ImageJ after the background signal intensity was normalized to the pre-bleaching intensity.

For eEF2/eEF1A: After transfecting the cells with EEF2-sfGFP or EEF1A-sfGFP plasmids and supplying NH_4Cl, the light-induced foci or the cytoplasmic region (if no foci were formed in the cells) were bleached by 405 nm laser and the fluorescence recovery was monitored. Cytoplasm was bleached longer because of its faster recovery. Fluorescence intensity was quantified using ImageJ after the background signal intensity was normalized to the pre-bleaching intensity.

Western-blot analysis

Cells were lysed in lysis buffer (1% Triton X-100 in PBS with 1% protease inhibitor (Roche, cat. no. 4693132001) and phosphatase inhibitors (Sigma, cat. no. P5726) for 30min at 4 °C. After centrifugation at 20,000 g for 15 min at 4 °C, the supernatant was mixed with 4× NuPAGE™ LDS Sample Buffer (ThermoFisher Scientific, cat. no. NP0008) and boiled for 5 min at 95 °C. Proteins were separated by 10% SDS-PAGE gel electrophoresis and transferred to a PVDF membrane (BIO-RAD, cat. no. 1620177). The membrane was blocked and incubated at 4 °C

overnight with the primary antibodies. After extensive washing in TBS with 0.3‰ Tween 20, the membrane was incubated with the secondary antibodies for 2 h at room temperature. Protein bands were visualized by chemiluminescence using the SuperSignal West Pico PLUS (ThermoFisher Scientific, cat. no. 34580) and detected using a ChemiDoc XRS system (BIO-RAD). The Quantity One v.4.6.2 (BIO-RAD) and ImageJ softwares were used for background subtraction and quantification.

Global protein synthesis measurement

Cells were plated in 6-well plate, washed, and then starved with methionine-free medium (DMEM (ThermoFisher Scientific, cat. no.21013-024) with 10% FBS and 1× GlutaMAX (ThermoFisher Scientific, cat. no. 35050-061)) for 1 h to deplete intracellular free methionine. L-AHA (Click Chemisry Tools, cat. no. 1066) was then added to label the cells at the final concentration of 50 μM for different time. After metabolic labeling, cells were washed and harvested. Protein concentration was measured by BCA Protein Assay Kit (Beyotime, cat. no. P0009) before Click reaction. Click reaction was performed using Click-&-Go™ Click Chemistry Reaction Buffer Kit (cat. no. 1001) and Biotin-PEG4-Alkyne (Click Chemistry Tools, cat. no. 12 Click Chemistry Tools,66). The reaction mixes then underwent western-blot analysis using HRP-labeled Streptavidin (Beyotime, cat. no. A0303) and anti-Tubb (Abcam, cat. no. ab6046) or anti-Gapdh (Proteintech, cat.no. 60004).

Global protein synthesis imaging and analysis in the single cells

Cells were cultured and labeled by L-AHA for different time as described above. After metabolic labeling, cells were fixed with 4% PFA diluted in PBS for 15 min in the incubator and then performed click reactions using Click-&-Go™ Plus 555 Imaging Kit (Click Chemistry Tools, cat. no. 1317). After DAPI staining, fluorescence signals were measured and analyzed for each cell by Operetta CLS High-Content System (PerkinElmer).

Luciferase reporter mRNA translation assay

Cells were seeded on the 96 well plate at a density of 1×10^4 cells per well. 500 ng capped renilla luciferase mRNAs, which were transcribed *in vitro* (ThermoFisher Scientific, cat. no. AM1344) from pRL-CMV Vector (Promega, cat. no. E2261), were transfected into each well along with 2 μl lipofectamine 2000 (ThermoFisher Scientific, cat. no. 11668). After different translation time, cells were lysed using Renilla Luciferase Assay System (Promega, cat. no. E2810) following the

instructions. After adding Renilla Luciferase Assay Reagent, luminescence was measured by a microplate luminometer (PerkinElmer Envision).

***In vitro* translation assay**

Rabbit reticulocyte lysates (ThermoFisher Scientific, cat. no. AM1200) were used to investigate the inhibition of translation by $(CAG)_n$ RNAs. $(CAG)_n$ RNAs were transcribed using T7 High Yield RNA Synthesis Kit (Apebio, cat. no. K1047), while the renilla luciferase mRNAs were transcribed using the same manner but supplemented with EZ Cap™ Reagent AG (Apebio, cat. no. B8176). Each aliquot of 12 μL reaction mixture contained 50% Retic Lysate, 6.25% 20× Translation Mix (-Met), 50 mM Met, 5% RiboLock RNase Inhibitor (ThermoFisher Scientific, cat. no. EO0382), 0.2 mM GTP, 0.2 mM ATP, 2 mM DTT, 50 nM $(CAG)_n$ RNA and 1.25% nanoluciferase substrate (Promega, cat. no. E2810) and 100 nM recombinant purified eEF2 protein or 2 μM BIND peptide. Reaction mixtures were incubated at 30 °C in 384-well plates for 5 min with the indicated RNA and/or proteins inside the SYNERGY neo2 microplate reader (Biotek). 3 μL Renilla luciferase mRNA was then added to each well to the final concentration of 5 nM. Translation reactions were incubated at 30 °C for 20 min. In the meanwhile, the luminescence from each well was continuously measured by the microplate reader to record the time course of protein synthesis. The recombinant eEF2 and eEF1A proteins used for the in vitro experiments (Fig. 4e, Extended Fig. 8) were purified from mammalian HEK293T cells. The eEF2 or eEF1A cDNAs were cloned to a modified pTT plasmids and were transfected to HEK293T cells using polyethylenimine (PEI, from Life iLab Biotech, cat. no. AC04L092). After cultured at 33 °C for 48 h, cells were harvested by centrifugation (400 g) at 4 °C for 3 min. The cell pellets were suspended in 50 mM Tris-HCl buffer, pH 7.5, with 150 mM NaCl, 20 mM Imidazole, 5% Trehaose, 25 U/mL benzonase, 0.5% w/v CHAPS, 1% Triton X-100 and 5% glycerol. Cells were then lysed by sonication, followed by centrifugation (3,000g) at 4 °C for 30 min. The supernatants were then loaded onto a HisTrap HP column (GE Healthcare, cat. no. 17524701), and eluted with 50 mM Tris-HCl buffer, pH 7.5, containing 150 mM NaCl, 5% glycerol and 300 mM imidazole. The indicated fractions were collected for experiments. The products were validated by coomassie blue staining. BIND and BIND-S synthesis were custom purchased from KS-V Peptide, and the peptides purity was measured by chromatography (98 %) and sequence validated by MASS-spectrum.

RT-qPCR

Total RNA was extracted using RNAsimple Total RNA Kit (Tiangen, cat. no. DP419). First-strand cDNA was then synthesized using FastQuant RT Kit (Tiangen, cat. no. KR106). All primers employed in RT-PCR were designed to recognize different exons of the target genes (including *18s,28s,45s, HTT and LAMP2*) in order to eliminate possible DNA contamination (sequences provided in Supplementary Table 1). Quantitative PCR was performed using SYBR Green Realtime PCR Master Mix (Toyobo, cat. no. QPK-201) by Mx3000P (Agilent Technologies). Primers targeting 7SK RNA or Hprt were used for normalization.

Polysome profiling analysis

Sucrose gradients (15% to 45% [wt/vol]) in gradient buffer (10 mM Tris [pH 7.4], 5 mM $MgCl_2$, 100 mM KCl, 2 mM DTT) were prepared in 13.5 mL ultracentrifuge tubes (Beckman, cat. no. 344059). Cells were incubated with medium containing 2 μg/mL Harringtonine (Selleck, cat.no. S9063) for 3min for transcription inhibition assay, and then incubated with medium containing 100 μg/mL CHX subsequently. For the standard assays, directly incubate the cells with CHX for 15 min and collect the cells. After the pre-treatment, the cells were washed with ice-cold PBS containing 100 μg/mL CHX. The cell pellet was collected and lysed in polysome lysis buffer: 10 mM Tris (pH 7.4), 5 mM $MgCl_2$, 100 mM KCl, 1% Triton X-100, 2 mM DTT, 100 U/mL RNase inhibitor, containing protease inhibitor and phosphatase inhibitors. Total UV Absorbance at 254 nm (A254) of each sample was measured and would be used for later normalization. The cell lysates were loaded onto the top of sucrose gradient and centrifuged at 35,000 rpm for 3.5 h at 4 °C in the SW41 Ti rotor (Beckman, cat.no. 331336). The centrifuged sample was fractionated while scanning at A254 to visualize the indicated ribosomal species using Biocomp Gradient Station. Polysome-to-monosome (P/M) ratios were calculated by comparing the areas under the 80S and polysome peaks. Gradient fractions were TCA precipitated and underwent western-blot analysis using indicated antibodies.

Ribosome run-off assay

Mouse striatal cells were plated in T75 flasks before treatment, and then incubated with 2 μg/mL of harringtonine for 3 min prior to CHX treatment. The cells were immediately incubated with CHX (100 μg/mL) for 15 mins and then collected. Polysome profiling analysis for each sample was performed as described above.

Surface sensing of translation (SUnSET)

Experiments were performed similarly as previously described[5]. The cells were incubated with 10 μg/mL puromycin (Sigma-Aldrich, cat. no. P7255) for 10 min, then harvested for western-blot analysis. 20 μg of proteins were loaded onto Bis-Tris protein gels (ThermoFisher Scientific, cat. no. NP0336BOX) prior immunoblotting by anti-puromycin antibody (DSHB, cat.no. PMY 2A4) and chemiluminescence.

SUnSET-based Ribosome Speed of Elongation (SunRiSE)

Experiments were performed similarly as previously described[6]. STHdh cells were seeded into T25 flasks. Each flask was treated with 2 μg/mL Harringtonine for different time slots at 33℃. Immediately after that, cells were incubated with 10 μg/mL puromycin (Sigma, cat. no. P7255). After puromycin treatment, cells were washed in cold PBS and fixed/permeabilized with Fixation/Permeabilization Solution Kit (BD Biosciences™, cat. no. 554714), following the manufacturer's instructions. After that, cells were stained for 1 h at 4°C with Alexa Fluor 488-conjugated anti-puromycin (1:100, Merck, cat. no. MABE343) in Perm Wash buffer. Flow cytometry was conducted by BD FACSCalibur (BD Biosciences™), and data were analyzed with FlowJo.

Transmission electron microscopy

Mouse striatal cells were cultured and harvested. The cells were then fixed with 2.5% (vol/vol) glutaraldehyde for 15 min and postfixed with 1% osmium tetroxide for 2–3 h. The samples were dehydrated by incubation in graded ethanol (50%, 70%, 90%, and 100%) and in propylene oxide for 10 min. After that, samples were embedded, sectioned, and stained with lead citrate. Images were captured using a Philips CM-120 TEM (Philips).

Visualization of nascent RNA

The capture of newly synthesized RNA in cells was conducted by Click-iT™ RNA Alexa Fluor™ 488 Imaging Kit (ThermoFisher Scientific, cat. no. C10329), following the manufacturer' instructions. Briefly, cells were cultured on coated cover slip in dishes, and labeled by 1 mM EU for 45 min or 90 min under normal cell culture conditions. For control groups, 5 μg/mL (final concentration) actinomycin-D (Sigma, cat. no. A9415) had been added into the culture medium for transcription inhibition purpose, 30 min prior to the EU labeling. After the EU labeling, cells were fixed using 3.7% formaldehyde in PBS and permeabilized by 0.5% Triton X-100. After Click reaction with Alexa Fluor 488 azide, the cells were stained with

Hoechst 33342 diluted in PBS (1:1000). After washing, fluorescence images were captured with a Zeiss LSM 880 microscope.

Immunohistochemistry of HD brain tissue sections

The post-mortem HD and control brain sections used in this study were obtained from the Brain UK and the Cambridge Brain Bank (Addenbrookes Hospital, Cambridge UK) supported by the NIHR Cambridge Biomedical Research Centre, with an appropriate ethical approval from the Brain UK (14/007). Paraffin-embedded HD brain tissue sections were baked in an oven for 1 hour at 62 ℃ to remove wax. The baked slides were then treated with xylene and 100% ethanol for 5 min twice, and washed with running water for 5 min, successively. After that, the slides were treated with 3% H_2O_2 in methanol for 30 min, and washed in running water for 5 min. Subsequently, they were heated in 1 L water containing 2.1 g citric acid (pH 6.0) in a microwave oven with the highest power for 30 min, cooled down in running water for 10 min, and rinsed in 1× TBS for 5 min.

Tissue section staining was carried out with Vectastain Elite ABC-HRP Kit (Peroxidase, Universal, Vector Laboratories, cat. no. PK-6200). Tissue sections were blocked with 5% normal horse serum (NHS) in 1× TBS with 0.05% Tween-20 (TBST) for 30 min at room temperature, followed by an additional 15 min blocking with avidin solution and a 15 min blocking with biotin solution (Avidin/biotin blocking kit, Vector Laboratories, cat. no. SP-2001). eEF2 primary antibody (Cell Signalling Technology, cat. no.2332) were diluted (1:100) in the blocking buffer (1× TBST with 5% NHS) and incubated with tissues overnight at 4°C. After washing for 2×5 min in 1× TBST, the tissue sections were incubated with the biotinylated second antibody (1:50) in the blocking buffer for 30 min at room temperature, followed by washing for 2×5 min in 1× TBST. Tissue sections were incubated with the avidin and biotinylated complex (prepared as instructed: 100 µL of avidin stock solution and 100 of biotinylated HRP stock solution were added to 5 mL 1× TBST buffer, and the mixture was kept at room temperature for 15–30 min before use) for 30 min, followed by 2×5 min washing with 1× TBST. Tissue sections were incubated with DAB (Vector Laboratories, cat.no. SK-4100) for 2 min. The nuclei were stained with haematoxylin (Sigma, cat. no. H9627) for 2 min. Finally stained tissue sections were treated with 100% ethanol for 2×5 min, and xylene for 2×5 min, successively, and cover-slipped with DPX mounting medium (Sigma, cat. no. 06522) in preparation for bright field microscopy using a Leica IM8 microscope.

RNA Fluorescence *In Situ* Hybridization (FISH)

STHdh cells treated with NH_4Cl (10 mM) for 48 h were fixed with 4% paraformaldehyde diluted in PBS for 15 min at room temperature, and then dehydrated with 50% (v/v), 70% and 100% ethanol for 5 min. They were then rehydrated with 70%, 50% ethanol for 2 min, followed by PBS for 10 min. The fixed cells were either used immediately, or stored in 100% ethanol at −20 °C until needed. RNA was probed by Cy3-labelled DNA oligonucleotides designed against CAG sequence (synthesized by GenePharma Technologies). Probe sequences were provided in Supplementary Table 1. Hybridization and wash buffers were purchased from GenePharma Technologies (cat. no. 1F12201) and used according to the manufacturer's protocol. Fluorescence images were captured with a Zeiss LSM 880 or an Olympus Fluoview FV3000 confocal microscope. RNA foci were analyzed with FIJI using a fluorescence-intensity and size-based threshold.

Simultaneous Visualization of RNA and Protein Targets

We combined the RNAScope ISH technology with immunofluorescence to spatially resolve RNA and protein targets simultaneously. RNAscope ISH was performed using RNAscope kit (Advanced Cell Diagnostics, cat. no. 323100). Probes targeting the mouse *Htt* mRNA (the target region was 3,898–4,826 nt; Advanced Cell Diagnostics, cat. no. 405881) together with the control probe (Advanced Cell Diagnostics, cat. no. 320871) were purchased. In brief, mice were anesthetized using a small animal anaesthesia machine (MSS-3, MSS International) by isoflurane (1.5% solution). Brains were immersion-fixed in fresh 4% PFA in PBS for 1 h and chilled sequentially in 10% (w/v), 20%, and 30% sucrose in PBS at 4 ℃. The brains were then embedded in OCT (Salura Finetek, cat. no. 4583), frozen by liquid nitrogen, and sectioned vertically at 10 μm thickness on a freezing microtome (Leica CM1950). The sections were mounted on superfrost plus microscope slides (Fisherbrand, cat. no. 12-550-15). Subsequent procedures were performed according to the RNA-Protein Co-Detection Ancillary Kit (Advanced Cell Diagnostics, cat. no. 323180) workflow. RNAscope Multiplex Fluorescent Kit v2 (Advanced Cell Diagnostics, cat. no. 323100) together with the Opal™ fluorophores (PerkinElmer, cat. no. FP1488001KT) was used to detect fluorescent ISH signals. Alexa Fluor 488-conjugated secondary antibody (ThermoFisher Scientific, cat. no. A21206) was used to detect eEF2 immunofluorescence. Fluorescence images were captured with a Zeiss LSM 880 or an Olympus Fluoview FV3000 confocal microscope.

In vitro phase-separation

$(CAG)_n$ RNAs labeled with Cy3-UTP and eEF2-sfGFP/eEF2-Alexa Fluor 488 purified proteins were dissolved in phase buffer (20 mM Tris pH7.4, 100 mM NaCl with 2% protease and phosphatase inhibitors). 4 μL of 20 μM protein were mixed with equal volume of 10 μM RNA and incubated in 384 well plate at 4°C overnight before imaging. The recombinant eEF2 protein was purified as indicated in the "*In vitro* translation assay" section. Labeled CAG RNAs were transcribed using HyperScribe™ T7 High Yield Cy3 RNA Labeling Kit (Apebio, cat. no. K1061).

Statistics

To ensure to reach a statistical power>0,8, power analyses were performed for each assay by NCSS-PASS (https://www.ncss.com/). Statistical comparisons between two groups were performed by unpaired two-tailed t tests. Statistical comparisons among multiple groups were conducted by one-way ANOVA tests and post-hoc tests for the indicated comparisons (Dunnett's tests for comparison with a single control, and Turkey's tests for comparison among different groups). Statistical comparisons for serials of data collected at different time points were conducted by two-way ANOVA tests. The similarity of variances between groups to be compared was tested when performing statistics in GraphPad Prism. Normality of data sets was assumed for ANOVA and t tests, and was tested by Shapiro-Wilk tests. When the data were significantly different from normal distribution, nonparametric tests were used for statistical analysis. The source data in excel files will be provided for all essential plots in the figures. The full gel blots will be provided as supplementary tables. All the other raw data are available from the authors upon request.

References for Material and Methods

1 Mizushima, N. *et al.* Dissection of autophagosome formation using Apg5-deficient mouse embryonic stem cells. *The Journal of cell biology* **152**, 657-668, doi:10.1083/jcb.152.4.657 (2001).

2 Shin, Y. *et al.* Spatiotemporal Control of Intracellular Phase Transitions Using Light-Activated optoDroplets. *Cell* **168**, 159-171 e114, doi:10.1016/j.cell.2016.11.054 (2017).

3 Zhang, Q. *et al.* A peptidylic inhibitor for neutralizing expanded CAG RNA-induced nucleolar stress in polyglutamine diseases. *RNA* **24**, 486-498, doi:10.1261/rna.062703.117 (2018).

4 Menalled, L. B., Sison, J. D., Dragatsis, I., Zeitlin, S. & Chesselet, M. F. Time course of early motor and neuropathological anomalies in a knock-in mouse model of Huntington's disease with 140 CAG repeats. *J Comp Neurol* **465**, 11-26, doi:10.1002/cne.10776 (2003).

5 Schmidt, E. K., Clavarino, G., Ceppi, M. & Pierre, P. SUnSET, a nonradioactive method to monitor protein synthesis. *Nat Methods* **6**, 275-277, doi:10.1038/nmeth.1314 (2009).

6 Arguello, R. J. *et al.* SunRiSE - measuring translation elongation at single-cell resolution by means of flow cytometry. *J Cell Sci* **131**, doi:10.1242/jcs.214346 (2018).

Extended Data Figures

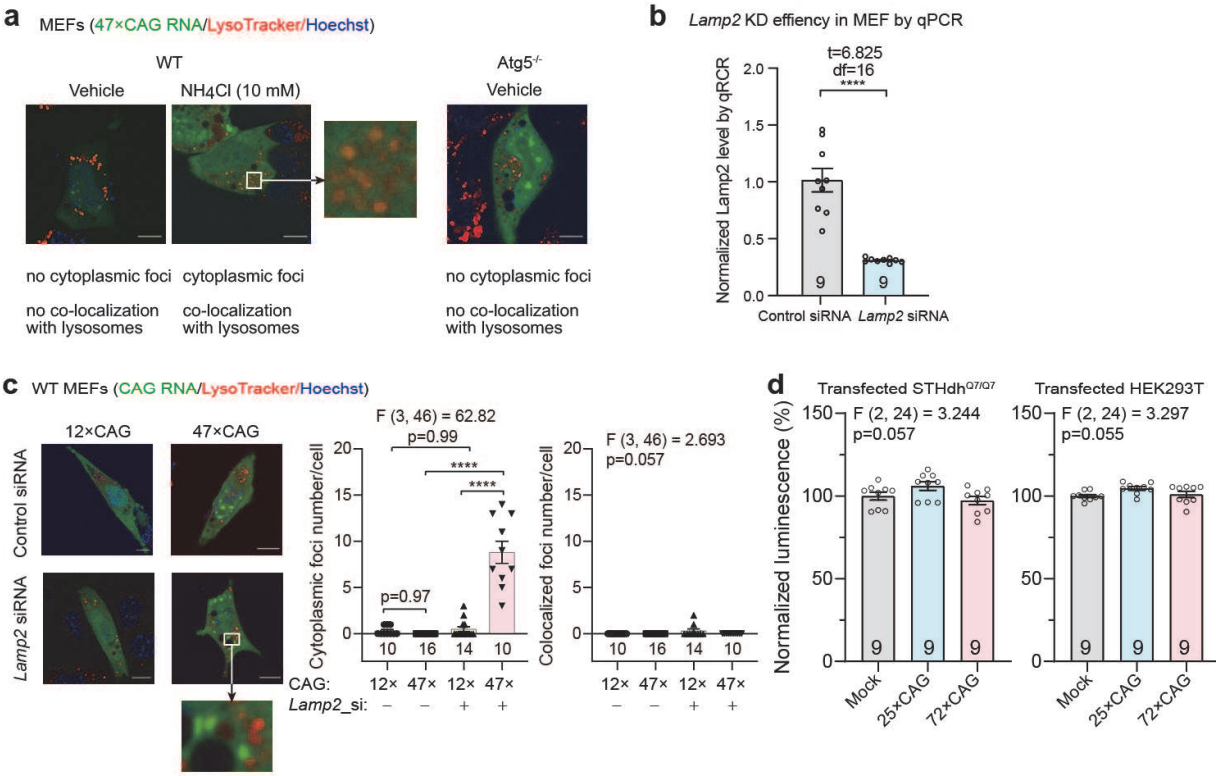

Extended Data Fig. 1. eCAGr RNA did not impact cell viability and its condensates were degraded by lysosomes *via* LAMP2. a. Representative images of eCAGr RNA foci (green, detected by MS2-GFP) and lysosomes (detected by LysoTracker) in the indicated cells. **b.** qPCR experiments confirming the knockdown of *Lamp2* mRNA. **c.** Representative images and quantifications showing that cytoplasmic eCAGr RNA foci were observed outside the lysosomes in cells when *Lamp2* was knocked-down. **d.** Cell viability measured by CellTiter-GLO assays for WT mouse striatal cells and HEK293T cells transfected with the indicated plasmids. Data are mean ± s.e.m.; analyzed by one-way ANOVA with multiple comparisons (**c & d**) or two-tailed unpaired t tests (**b**). n indicates independently repeated wells (**b & d**) or the number of cells (**c**). Scale bars, 10 μm (**a, c**).

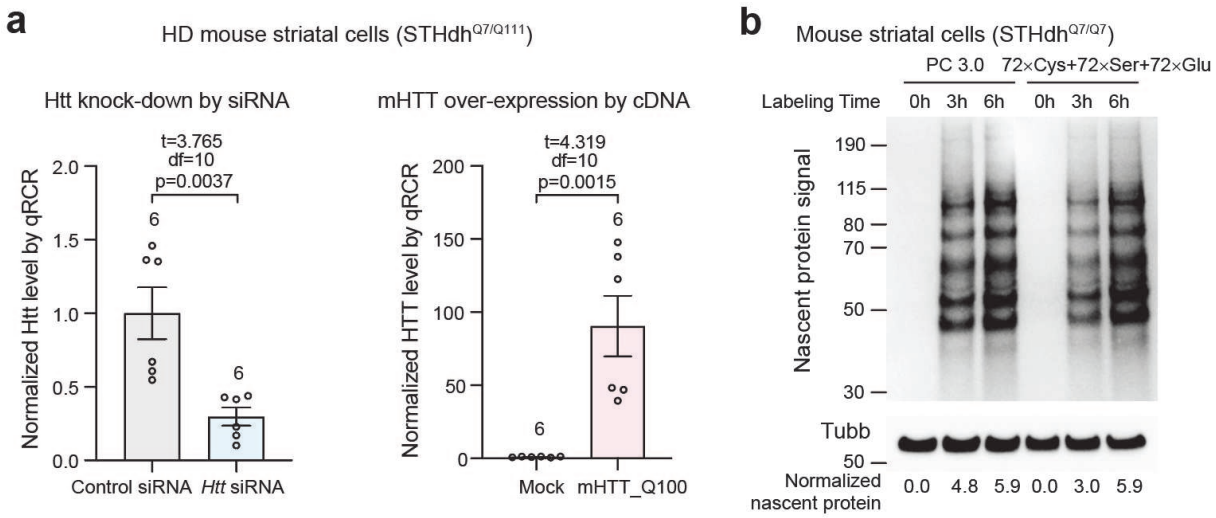

Extended Data Fig. 2. Control experiments for eCAGr RNA's effects on nascent protein synthesis. a. Plots for qPCR validation of the knock-down or over-expression of the indicated target RNAs in HD mouse striatal (STHdh$^{Q7/Q111}$) cells. The n number indicates independently repeated wells. **b.** Representative western-blots (from 3) of nascent proteins at indicated time points after metabolic labeling in WT mouse striatal cells transfected with plasmids expressing possible RAN translation products from the eCAGr RNA: 72×Cys, 72×Ser and 72×Glu. These plasmids were codon-optimized and the translation of these protein products was driven by the ATG start codon. Data are mean ± s.e.m.; analyzed by two-tailed unpaired t tests.

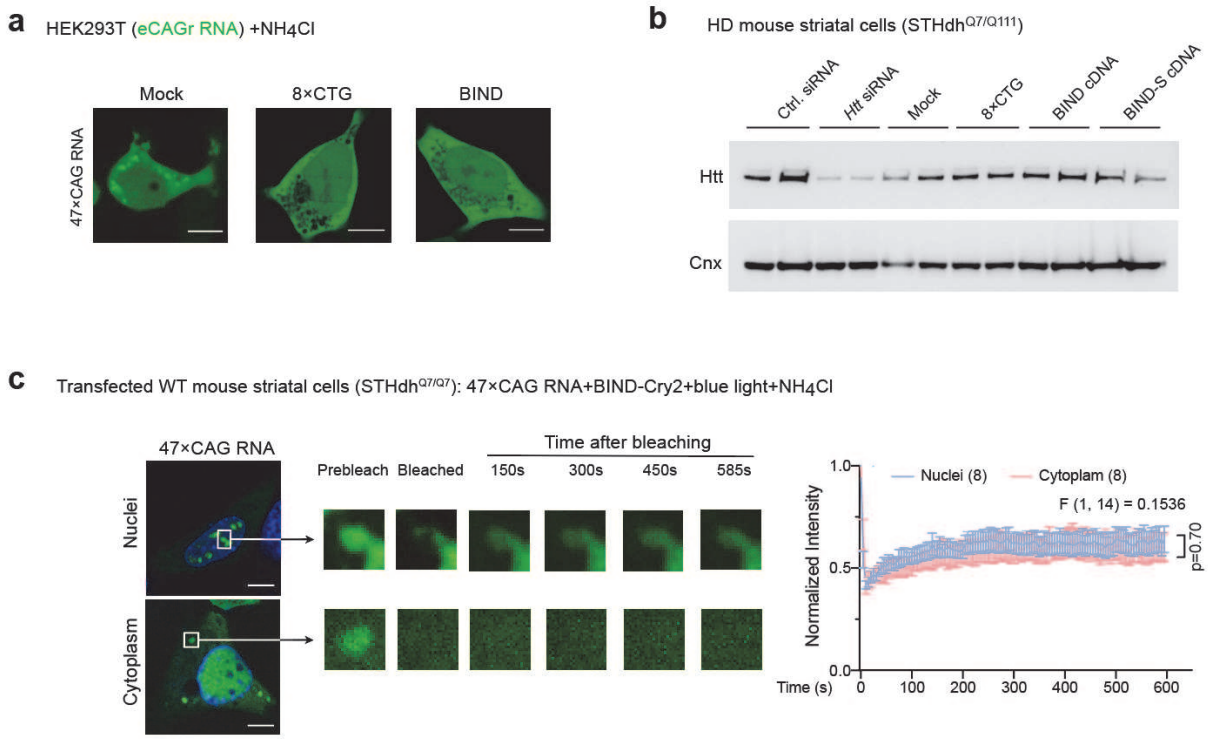

Extended Data Fig. 3: Control experiments for effects of BIND and 8×CTG on eCAGr RNA gelation. a. Representative images (from 6) of eCAGr RNA visualization in NH_4Cl-treated HEK293T cells expressing 47×CAG RNA together with MS2CP-YFP, upon co-transfection with the 8×CTG DNA oligo or the plasmid expressing the eCAGr RNA binding peptide BIND. **b.** Representative western-blots (from 3) of the Htt protein in HD ($Hdh^{Q7/Q111}$) mouse striatal cells transfected with the indicated siRNAs, 8×CTG DNA oligo, or the indicated cDNA plasmids. **c.** Representative FRAP images and quantifications showing the fluorescence recovery of nuclear/cytoplasmic eCAGr RNA foci in NH_4Cl-treated WT ($Hdh^{Q7/Q7}$) mouse striatal cells expressing 47×CAG RNA upon blue light stimulation. Little recovery was observed, indicating RNA gelation induced by blue light. Data are mean ± s.e.m.; analyzed by two-way ANOVA (**c**). The numbers of cells are shown in the plot (**c**). Scale bars, 10 μm (**a**, **c**).

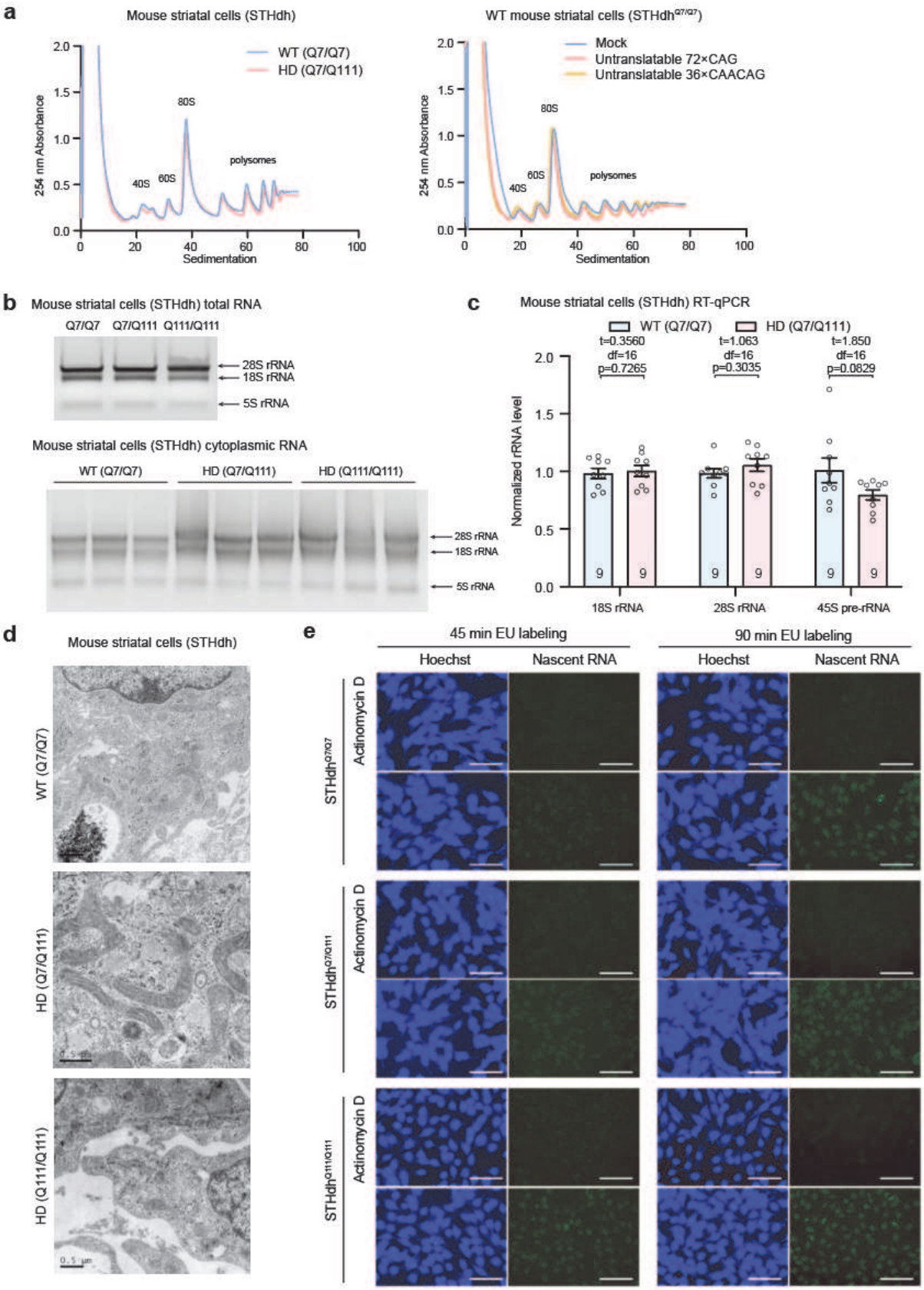
a
Mouse striatal cells (STHdh)
WT (Q7/Q7)
HD (Q7/Q111)
254 nm Absorbance
Sedimentation
40S
60S
80S
polysomes
WT mouse striatal cells (STHdh^Q7/Q7)
Mock
Untranslatable 72×CAG
Untranslatable 36×CAACAG
b
Mouse striatal cells (STHdh) total RNA
Q7/Q7
Q7/Q111
Q111/Q111
28S rRNA
18S rRNA
5S rRNA
Mouse striatal cells (STHdh) cytoplasmic RNA
WT (Q7/Q7)
HD (Q7/Q111)
HD (Q111/Q111)
c
Mouse striatal cells (STHdh) RT-qPCR
WT (Q7/Q7)
HD (Q7/Q111)
t=0.3560
df=16
p=0.7265
t=1.063
df=16
p=0.3035
t=1.850
df=16
p=0.0829
Normalized rRNA level
18S rRNA
28S rRNA
45S pre-rRNA
d
Mouse striatal cells (STHdh)
WT (Q7/Q7)
HD (Q7/Q111)
HD (Q111/Q111)
e
45 min EU labeling
90 min EU labeling
Hoechst
Nascent RNA
Actinomycin D
STHdh^Q7/Q7
STHdh^Q7/Q111
STHdh^Q111/Q111

Extended Data Fig. 4: The eCAGr RNA in mouse striatal cells did not affect ribosome biogenesis. a. Representative polysome profiles (from 8) of WT/HD mouse striatal cells or the WT striatal cells expressing indicated RNAs. **b.** Images of agarose gels for total/cytoplasmic RNA extracted from WT ($STHdh^{Q7/Q7}$) and HD ($STHdh^{Q7/Q111}$ and $STHdh^{Q111/Q111}$) mouse striatal cells. **c.** Plots for RT-qPCR quantifications of normalized 18S, 28S and 45S RNA levels in WT and HD mouse striatal cells. **d.** Representative electron microscope images (from 5) showing ribosome distribution and density in mouse striatal cells. Scale bars, 0.5 μm. **e.** Nascent RNA synthesis rates visualized by EU-labeling in WT and HD mouse striatal cells. The RNA synthesis blocker actinomycin-D-treated groups were tested to confirm the specificity of the signals. Scale bars, 100 μm. Data are mean ± s.e.m.; analyzed by two-tailed unpaired t tests (**c**). The independently repeated wells are shown in the plot (**c**).

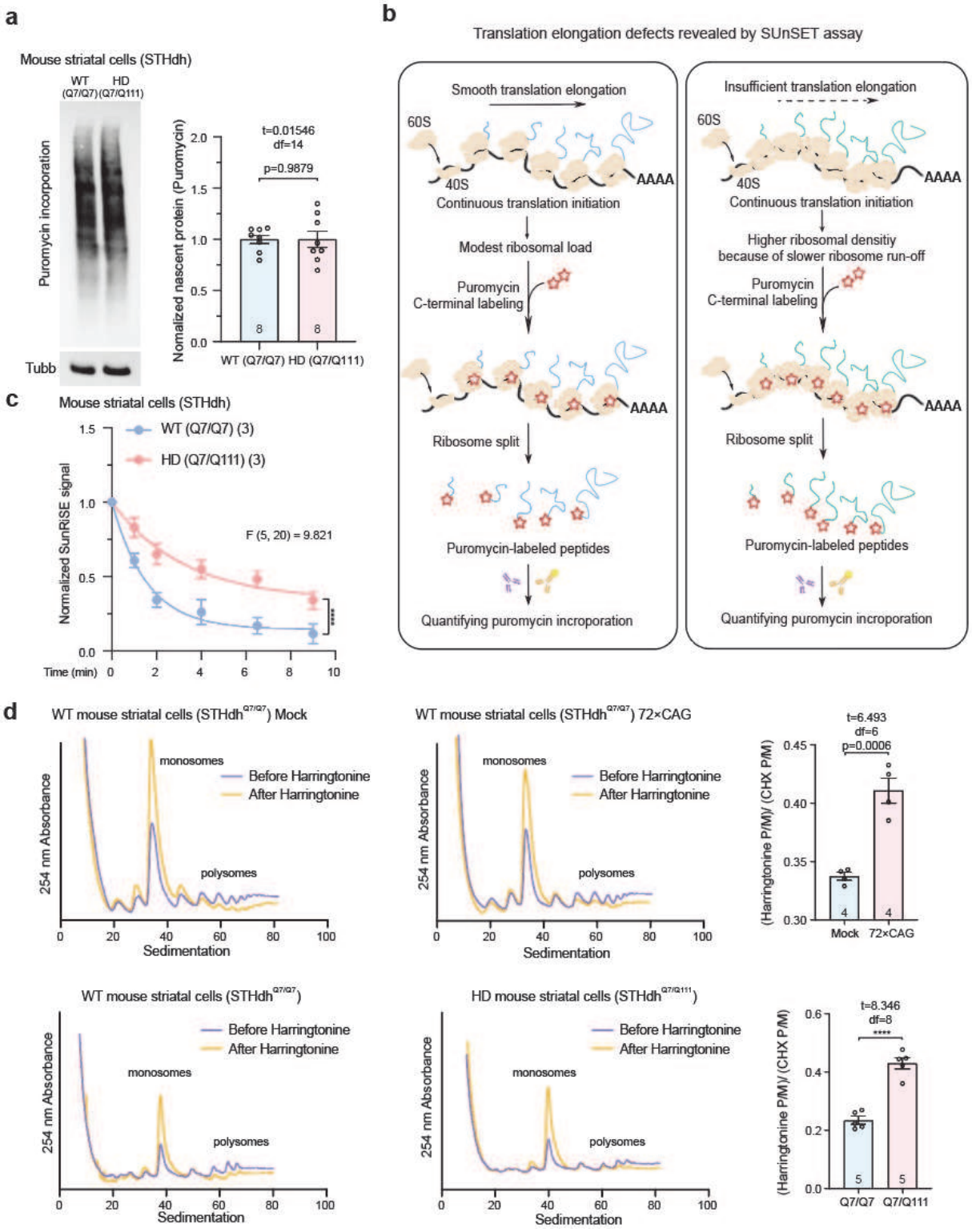

Extended Data Fig. 5: The eCAGr RNA impaired the protein translation elongation. a. Representative gel images and quantifications of puromycin-labeled proteins in WT and HD

mouse striatal cells in SUnSET assays. **b.** Schematic showing that the conventional SUnSET assay may not be able to reveal translation elongation defects. **c.** The plot of SunRiSE assay signals (detected by high-content imaging) showing a decrease of translation elongation in WT versus HD mouse striatal cells. **d.** Representative polysome profiles and quantifications of WT/HD mouse striatal cells or the transfected WT mouse striatal cells expressing 72×CAG RNA, before versus after ribosome run-off. The polysome-to-monosome (P/M) ratio was calculated for each plot, and ratio between the P/M after 3 min harringtonine treatment (Harringtonine P/M) and the P/M before harringtonine treatment (CHX P/M, treated with cycloheximide alone without pre-treatment of harringtonine for 3 min) was quantified for the run-off rate. Data are mean ± s.e.m.; analyzed by two-tailed unpaired t test (**a**, **d**) or two-way ANOVA (**c**). The numbers of independently repeated assays (**a**, **c**, **d**) are shown in each plot. ****: $p < 0.0001$.

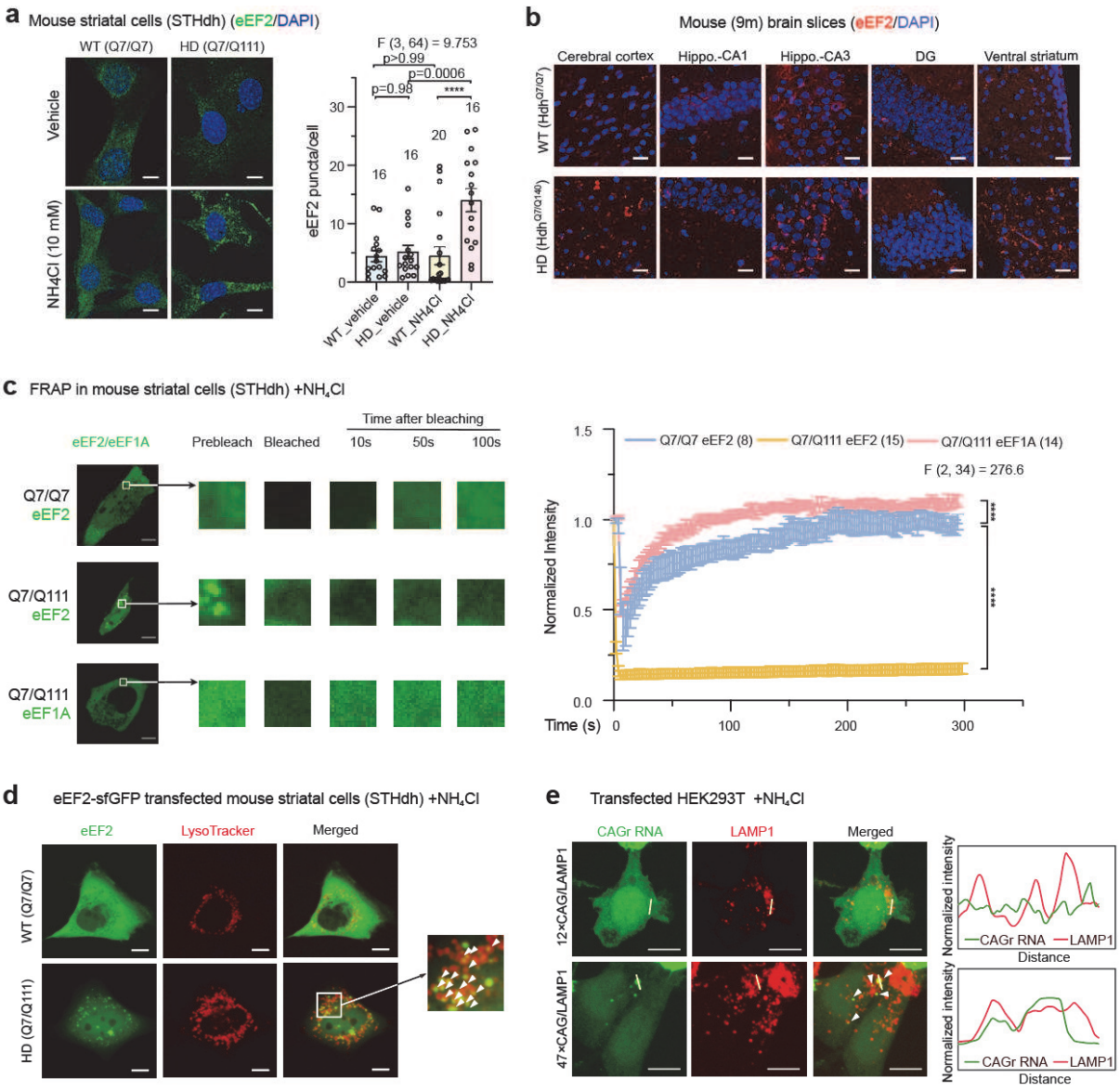

Extended Data Fig. 6: eEF2 formed condensates in eCAGr RNA-harboring cells. a. Representative images and quantifications of eEF2 condensates in WT versus HD mouse striatal cells treated with vehicle (culture medium) or the lysosome inhibitor NH_4Cl. **b.** Representative immunofluorescence images of diverse brain sections showing the eEF2 puncta in HD ($Hdh^{Q7/Q140}$) versus WT ($Hdh^{Q7/Q7}$) mice (9 m). The quantifications are presented in Fig. 4c. **c.** Representative images and quantifications of the FRAP experiments for cytoplasmic eEF2 or eEF1A in NH_4Cl-treated WT or HD mouse striatal cells. **d.** Representative images of eEF2-sfGFP and the lysosomes in NH_4Cl-treated WT or HD mouse striatal cells**.** Colocalizations of eEF2 foci and lysosomes are indicated by white arrows. **e.** Representative fluorescence images of

transfected eCAGr RNAs and LAMP1-mcherry in HEK293T cells treated with the lysosome inhibitor NH_4Cl. Colocalization patterns between eCAGr RNAs and LAMP1 at the beige lines are visualized. The colocalized condensates are also indicated by white arrows. Data are mean ± s.e.m.; analyzed by one-way ANOVA with multiple comparisons (**a**) or two-way ANOVA with multiple comparisons (**c**). The numbers of cells (**a** & **c**) are shown in each plot. ****: $p < 0.0001$. Scale bars, 10 μm (**a**-**e**).

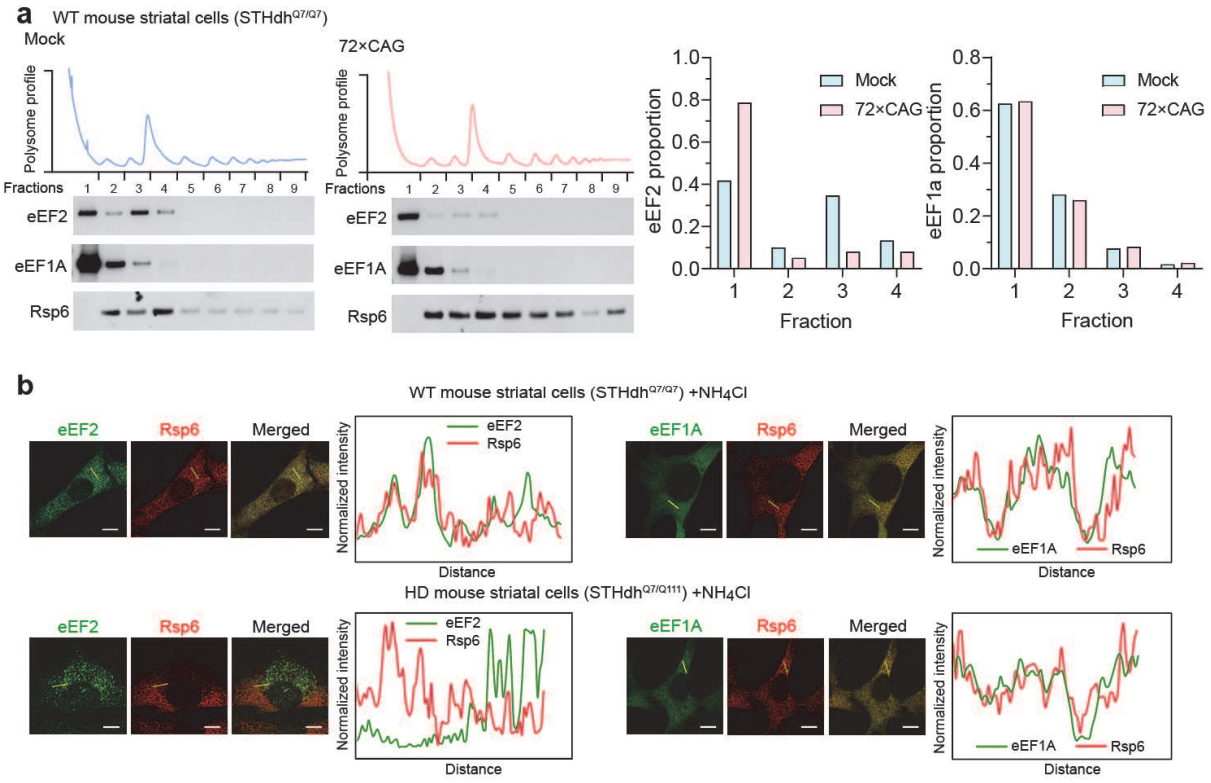

Extended Data Fig. 7: eEF2 showed weaker association with the ribosomes in eCAGr RNA-expressing cells. a. Representative western-blots (from 3) with the corresponding polysome profiles, together with the quantifications showing the distribution of eEF2 and eEF1A in the indicated polysome fractions of transfected WT mouse striatal cells expressing 72×CAG RNA versus the Mock control. **b.** Representative fluorescence images (from 8) of endogenous eEF1A, eEF2 and Rsp6 (a ribosome marker) in WT or HD mouse striatal cells treated with the lysosome inhibitor NH_4Cl. Colocalization patterns between eEF1A/eEF2 and Rsp6 at the yellow lines are visualized. The eEF2-Rsp6 colocalization was drastically impaired. Scale bars, 5 μm.

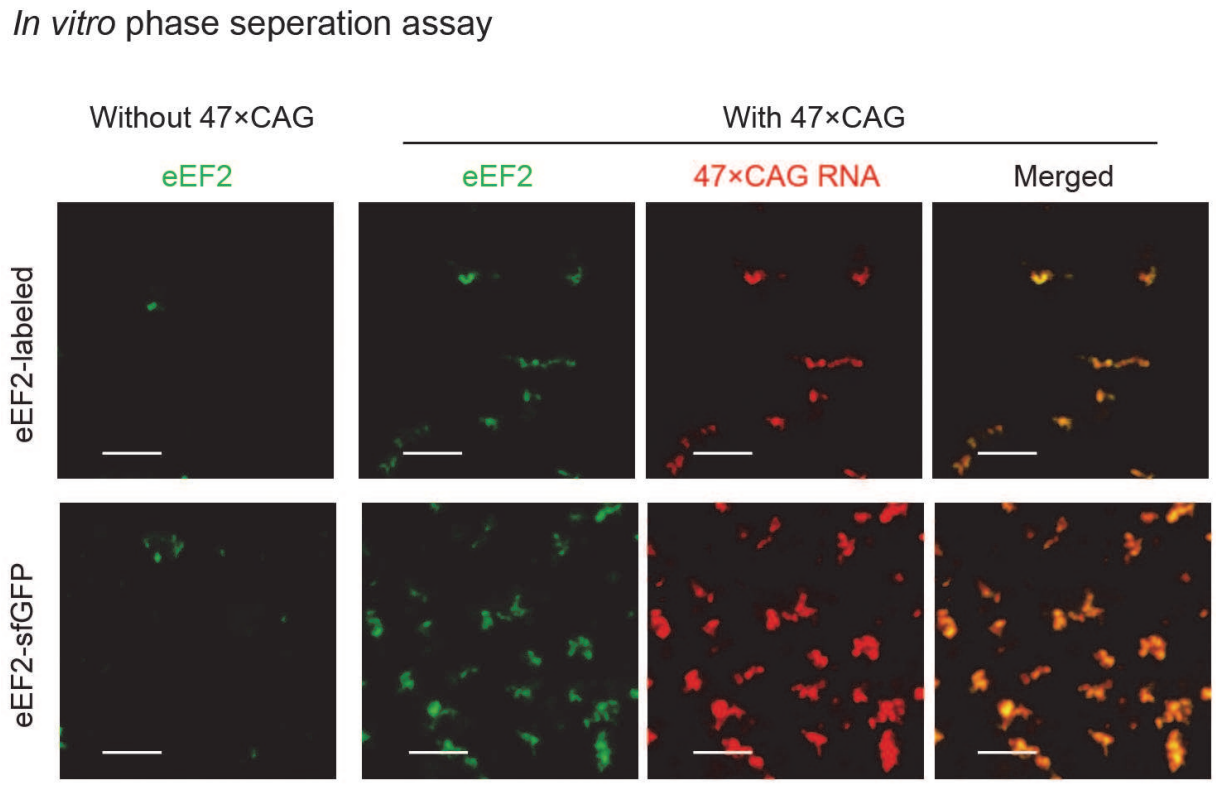

Extended Data Fig. 8: eEF2 forms gel-like condensates *in vitro.* Representative images (from 5) showing that fluorophore-labeled or sfGFP-tagged recombinant purified eEF2 proteins form gel-like condensates together with 47×CAG RNA *in vitro*. Scale bars, 5 μm.

5

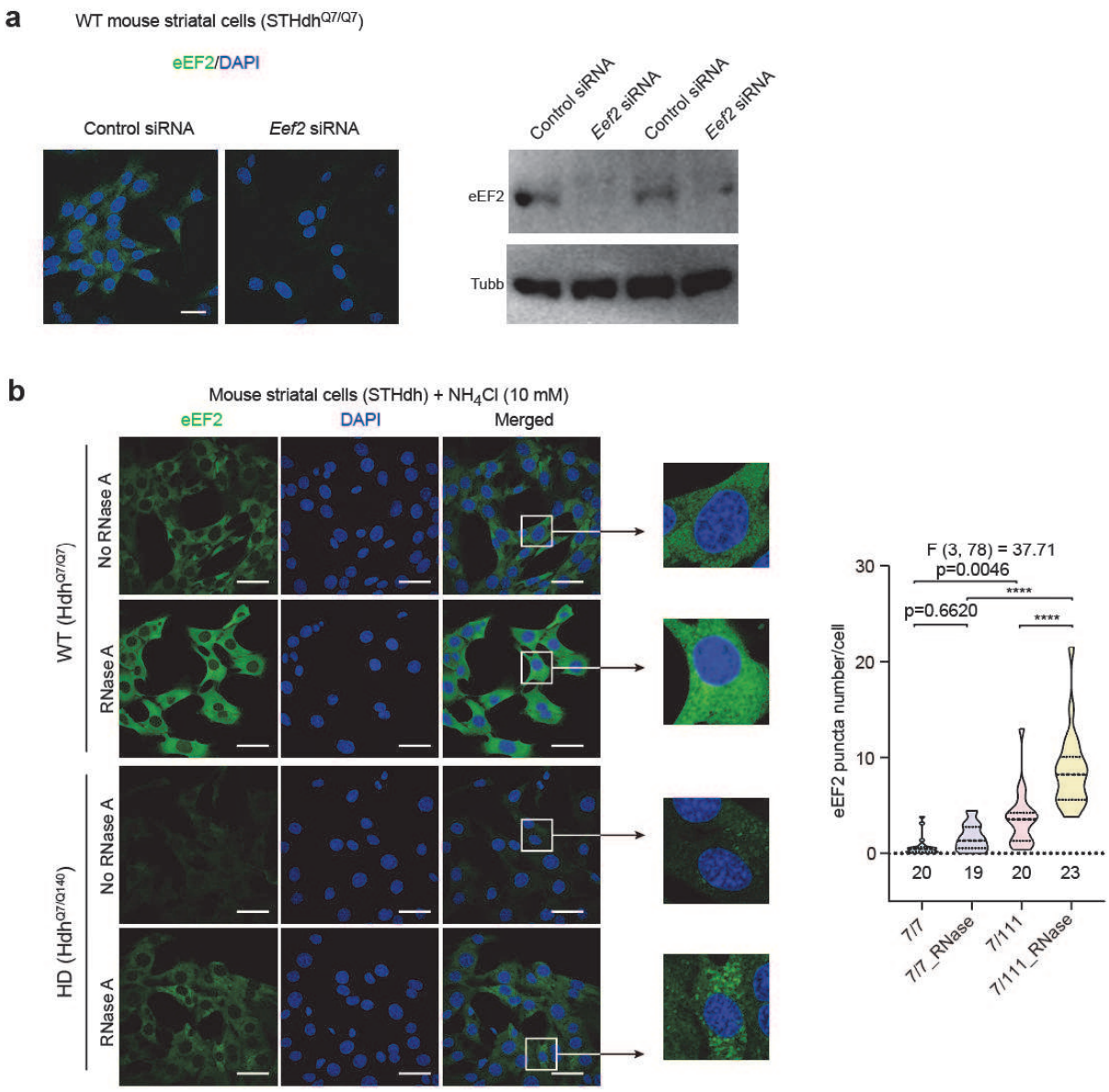

Extended Data Fig. 9: Control experiments for eEF2 staining. a. Representative images (from 3) and western-blots (from 3) showing the endogenous eEF2 in WT mouse striatal cells upon the knock-down of eEF2 by the siRNA, validating the antibody specificity. **b.** Representative images and quantifications of eEF2 puncta in NH_4Cl-treated WT or HD mouse striatal cells with or without RNase A treatment after fixation and prior to the staining. The RNase treatment specifically increased eEF2 puncta in the HD cells, suggesting that eCAGr RNAs may mask the epitopes of some of the eEF2 puncta. Data are mean ± s.e.m.; analyzed by one-way ANOVA with multiple comparisons. The numbers of cells analyzed are shown in the plot. ****: $p < 0.0001$. Scale bars, 30 μm.

Extended Video 1. A representative video showing different recover rates of the eCAGr RNA foci in the nucleus versus cytoplasm in the same cell in a FRAP experiment.

Supplementary Files

This is a list of supplementary files associated with this preprint. Click to download.

- SupplementaryFigs.pdf
- 3968851dataset3664932qt89n3.xlsx